Differences in vertical and horizontal transmission dynamics shape plasmid distribution in clinical enterobacteria

Aida Alonso-del Valle[#,1,*], Laura Toribio-Celestino[#,1], Anna Quirant[2], Carles Tardio Pi[3,4], Javier DelaFuente[1], Rafael Canton[5,6], Eduardo Rocha[7], Carles Ubeda[2,8], Rafael Peña-Miller[3], Alvaro San Millan[1,8,*].

Affiliations

1. Centro Nacional de Biotecnología (CNB), CSIC. Madrid, Spain.
2. Fundación para el Fomento de la Investigación Sanitaria y Biomédica de la Comunitat Valenciana - FISABIO, Valencia, Spain.
3. Centro de Ciencias Genómicas, Universidad Nacional Autónoma de México, Cuernavaca, Mexico.
4. Instituto de Investigaciones en Matemáticas Aplicadas y en Sistemas, Unidad Académica Yucatán, Universidad Nacional Autónoma de México, Yucatán, México.
5. Servicio de Microbiología. Hospital Universitario Ramón y Cajal-IRYCIS. Madrid, Spain.
6. Centro de Investigación Biológica en Red de Enfermedades Infecciosas (CIBERINFEC), Instituto de Salud Carlos III, Madrid, Spain.
7. Institut Pasteur, Université de Paris Cité, CNRS UMR3525, Microbial Evolutionary Genomics, Paris, France.
8. Centro de Investigación Biológica en Red de Epidemiología y Salud Pública (CIBERESP), Instituto de Salud Carlos III, Madrid, Spain.

# Contributed equally

* Correspondence and request for materials should be addressed to Aida Alonso-del Valle (aalonso@cnb.csic.es) & Alvaro San Millan (asanmillan@cnb.csic.es).

Abstract

Conjugative plasmids can transfer both vertically and horizontally in bacterial communities, playing a key role in the dissemination of antimicrobial resistance (AMR) genes across bacterial pathogens. AMR plasmids are widespread in clinical settings, but their distribution is not random, and certain associations between plasmids and bacterial clones are particularly successful. However, knowledge remains limited about the contribution made by vertical and horizontal transmission dynamics to plasmid distribution and maintenance in clinically relevant bacterial communities. In this study, we used a collection of wild type enterobacterial strains isolated from hospitalized patients to perform a comprehensive analysis of the transmission dynamics of the globally spread carbapenem resistance plasmid pOXA-48. We combined *in vitro* and *in vivo* experimental approaches to quantify key traits responsible for vertical (the level of AMR) and horizontal (conjugation frequency) plasmid transmission. Our results reveal significant variability in these traits across different bacterial hosts, with *Klebsiella* spp. strains showing higher pOXA-48-mediated AMR and conjugation frequencies than *Escherichia coli* strains. Using experimentally determined parameters, we developed a simple mathematical model to interrogate the contribution of vertical and horizontal transmission to plasmid distribution in bacterial communities. These simulations revealed that a small subset of clones, combining high vertical and horizontal plasmid transmission ability, play a critical role in stabilizing the plasmid in different polyclonal microbial communities. Our results indicate that strain-specific differences in plasmid transmission dynamics dictate successful associations between plasmids and bacterial clones, shaping AMR evolution.

Significance statement

Conjugative plasmids are the main vehicle for the dissemination of AMR genes across many bacterial pathogens, contributing to one of the most concerning public health problems facing modern societies. Understanding the rules governing plasmid dynamics is therefore crucial to controlling the global AMR crisis. In this study, we show that the plasmid-associated traits responsible for vertical and horizontal plasmid transmission in bacterial communities vary across different bacterial hosts. This information can be used to predict which specific plasmid-bacteria associations are more likely to spread in bacterial communities, thus enabling health care authorities to predict, and potentially control, the evolution of AMR in clinical settings.

55 **Introduction**

56 Plasmids shape bacterial ecology and evolution by spreading accessory genes across
57 populations. Plasmids can disseminate both vertically and horizontally. Vertical transmission is
58 coupled to the division of the bacterial host, whereas horizontal transmission is mediated mainly
59 by conjugation (the direct cell-to-cell transfer of plasmids through a bridge-like connection) (1).
60 Vertical plasmid transmission is favored in the presence of environmental stresses that select for
61 plasmid-encoded genes, but in the absence of plasmid-specific selection, vertical transmission is
62 usually hindered by the fitness costs that plasmids produce in their bacterial hosts (2, 3).
63 Therefore, plasmids' interests can align or conflict with those of their bacterial hosts depending
64 on the environmental conditions, leading to complex eco-evolutionary dynamics (4-6). Horizontal
65 plasmid transmission can in principle make up for a deficit in vertical transmission, although
66 conjugation rates vary considerably depending on the plasmid type (7, 8). The fate of plasmids in
67 bacterial populations is thus determined by the interplay between horizontal and vertical
68 transmission dynamics (and their evolution) (9-12). Multiple theoretical and experimental studies
69 have investigated plasmid dynamics in clonal bacterial populations (7, 8, 13-17). However,
70 information is very limited about how vertical and horizontal plasmid transmission dynamics vary
71 across the diversity of wild type bacteria that plasmids encounter in natural communities and how
72 this variability may affect plasmid distribution in complex microbiota (18-21).

73 A dramatic example of the ability of plasmids to fuel bacterial evolution is the central role they
74 play in the spread of antimicrobial resistance (AMR) in clinical pathogens, which is one of the
75 most urgent public health threats facing humanity (22, 23). One particularly concerning group of
76 drug resistant pathogens is carbapenemase-producing enterobacteria (order *Enterobacterales*),
77 which appear on the WHO "priority pathogens" list (24, 25). Carbapenemases are β-lactamase
78 enzymes able to degrade carbapenem antibiotics and are mainly acquired through conjugative
79 plasmids (22). pOXA-48-like plasmids (from here on pOXA-48) constitute one of the most
80 clinically important groups of carbapenemase-producing plasmids (26). pOXA-48 is a broad-host-
81 range conjugative plasmid from the plasmid taxonomic unit L (27) that encodes the OXA-48
82 carbapenemase and is disseminated across enterobacteria worldwide (26). Like most AMR
83 plasmids, pOXA-48 is not randomly distributed across bacterial hosts, and, although it has a broad
84 potential host range, it is strongly associated with *Klebsiella pneumoniae* and is especially

85 prevalent in high-risk clones of specific sequence-types (ST), such as ST11 or ST101 (28, 29). In
86 a previous study, we proposed that this bias in host distribution could be explained in part by
87 pOXA-48-associated fitness costs in the absence of antibiotics (30). However, an analysis of the
88 distribution of pOXA-48 fitness effects across a collection of *Escherichia coli* and *Klebsiella* spp.
89 clinical strains revealed that, although pOXA-48 produced a wide distribution of fitness effects
90 across these hosts, these effects could not explain overall plasmid distribution, especially at the
91 species level (30).

92 In the present study, we performed a comprehensive analysis of vertical and horizontal pOXA-48
93 transmission dynamics across clinical enterobacteria, using multidrug resistant *E. coli* and
94 *Klebsiella* spp. strains isolated from the gut microbiota of hospitalized patients at a large hospital
95 in Madrid, Spain (Ramon y Cajal University Hospital). Through a combination of *in vitro* and *in*
96 *vivo* experimental approaches, we demonstrate that (i) pOXA-48 confers a higher level of AMR
97 in *Klebsiella* spp., and that (ii) *Klebsiella* spp. strains are, on average, more permissive than *E.*
98 *coli* strains to pOXA-48 acquisition through conjugation. Integration of these new experimentally
99 determined parameters with our previous data in a simple population dynamics model allowed us
100 to interrogate how plasmid transmission dynamics determine the distribution of plasmid pOXA-48
101 across clinical enterobacteria.

102 **Results**

103 **Experimental system**

104 In this study, we used a collection of multidrug-resistant clinical enterobacterial strains isolated
105 from the gut microbiota of patients at a large hospital in Madrid. We focused on the two most
106 prevalent species associated with pOXA-48 in this hospital, *K. pneumoniae* and E*. coli* (28). Since
107 *K. quasipneumoniae* and *K. variicola* (two species previously misidentified as *K. pneumoniae*) are
108 also associated with pOXA-48 in the hospital (28), we included strains from these species in the
109 study. From now on we use *Klebsiella* spp. to refer to the strains in our collection belonging to
110 these three *Klebsiella* species.

111 To analyze pOXA-48 transmission dynamics it is necessary to work with pOXA-48-free strains,
112 which are able to receive the plasmid by conjugation. Therefore, we selected 25 *Escherichia coli*
113 and 25 *Klebsiella* spp. pOXA-48-free strains representative of the phylogenetic diversity of these

114 species in our hospital, and sequenced their genomes (Fig. S1 and Table S1, collection partially
115 overlapping with the one in ref. (30), see Methods). Although these strains were pOXA-48-naive,
116 they were identified as ecologically compatible with pOXA-48 because they were obtained from
117 patients on hospital wards where pOXA-48-carrying enterobacteria were commonly isolated from
118 other patients during the same period (28).

119 **AMR level conferred by pOXA-48 in wild type enterobacteria**

120 To characterize pOXA-48 vertical transmission dynamics in the presence of antibiotics, we
121 determined the impact of plasmid acquisition on the level of AMR. pOXA-48 was introduced by
122 conjugation into the pOXA-48-naive enterobacteria collection. Four *E. coli* strains and one *K.*
123 *pneumoniae* strain were unable to acquire the plasmid, and whole genome sequencing of the
124 remaining transconjugants revealed pOXA-48 mutations in six *E. coli* and six *Klebsiella* spp.
125 transconjugants. After excluding these strains, we used the remaining 15 *E. coli* and 18 *Klebsiella*
126 spp. isogenic strains pairs with or without pOXA-48 plasmid for this analysis (Fig. S1). For each
127 of the transconjugant (TC) and plasmid-free (PF) clones, we determined the minimal inhibitory
128 concentration (MIC) of 4 clinically important β-lactam antibiotics: amoxicillin in combination with
129 the β-lactamase inhibitor clavulanic acid (AMC) and the carbapenems ertapenem (ERT),
130 imipenem (IMP), and meropenem (MER) (Fig. 1A). Compared with *E. coli*, *Klebsiella* spp. strains
131 showed higher constitutive resistance to all four antibiotics (Wilcoxon rank sum test: AMC, W =
132 47.5, P = 0.001; ERT, W = 14.5, P = 8.68 x 10^{-6}; IMP, W = 15, P = 5.16 x 10^{-6}; MER, W = 56, P =
133 0.002), as well as higher resistance level after plasmid acquisition (Wilcoxon rank sum test: AMC,
134 W = 27, P = 8.94 x 10^{-5}; ERT, W = 82, P = 0.031; IMP, W = 29.5, P = 4.79 x 10^{-5}; MER, W = 54,
135 P = 0.002).

136 The diverse genomic background and AMR gene content of the strains under study made it
137 difficult to elucidate a genetic origin for the higher AMR levels reached by pOXA-48-carrying
138 *Klebsiella* spp. (Fig. S2). However, a prominent influence on plasmid-mediated AMR level is
139 plasmid copy number (PCN). AMR level commonly escalates with PCN for AMR mechanisms
140 showing strong gene dosage effects, such as carbapenemases (31, 32). We used the genome
141 sequencing data to estimate pOXA-48 PCN in the strains under study (Fig. 1B). The results
142 showed that PCN was higher in *Klebsiella* spp. (mean = 2.21, SD = 1.53) than in *E. coli* strains
143 (mean = 1.41, SD = 0.55) (Wilcoxon rank-sum test, W = 76, P = 0.03). We then compared pOXA-

144 48 PCN and AMR levels for the antibiotic to which pOXA-48 confers the highest level of
145 resistance: AMC (average fold-change in MIC associated to pOXA-48 presence = 244.7). The
146 final AMC resistance level correlated positively with PCN in the strains under study (Spearman's
147 correlation: $R = 0.5$, $P = 0.003$; Fig. S3), supporting the idea that the higher PCN is at least partly
148 responsible for the elevated AMR level in *Klebsiella*. spp. Finally, to investigate if the differences
149 in PCN were also present in strains naturally carrying pOXA-48, we used the same genomic
150 approach to analyze PCN in a recently characterized large collection of 200 pOXA-48-carrying
151 clinical isolates from the same hospital. In line with the results from the transconjugant strains,
152 PCN was higher in *Klebsiella* spp. (mean = 2.35, SD = 0.88) than in *E. coli* (mean = 1.46, SD =
153 1.33) (Fig. 1C; Wilcoxon rank-sum test, $W = 1271$, $P = 1.32 \times 10^{-14}$).

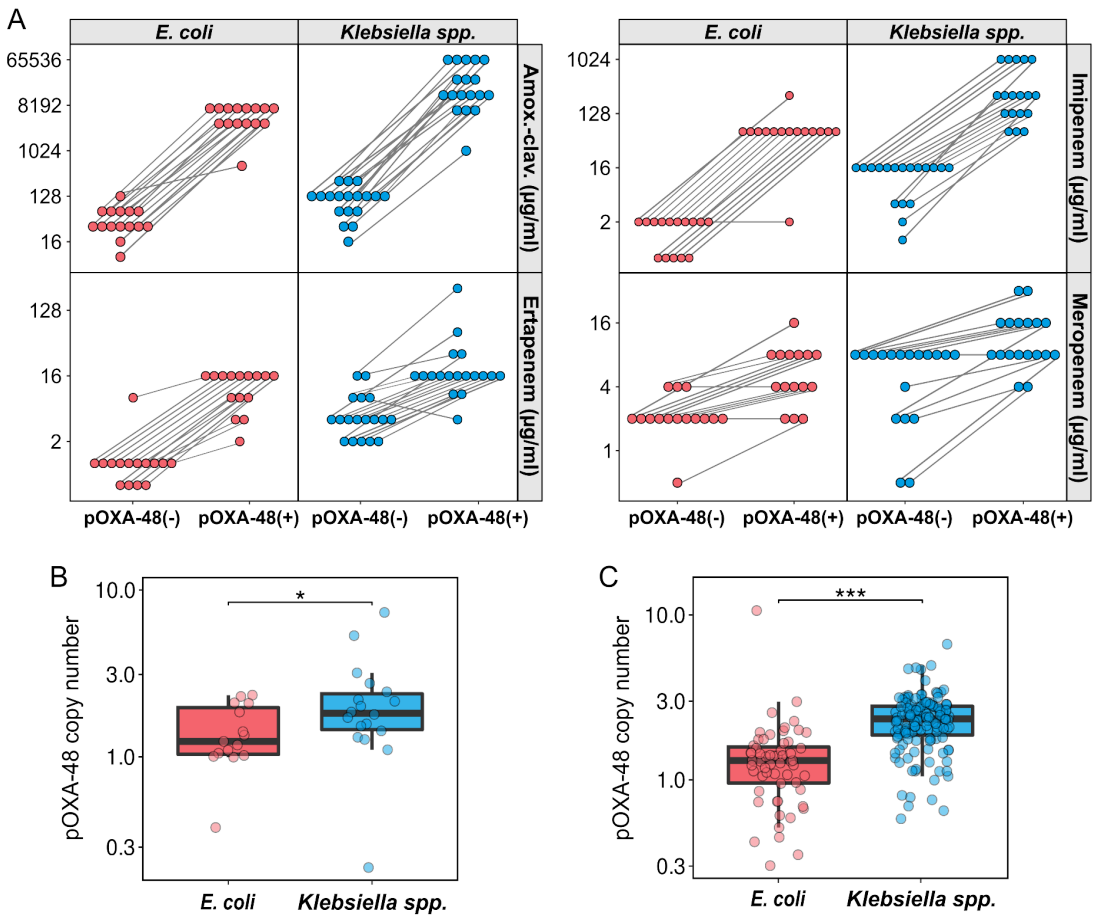

154

155 **Fig. 1. Resistance levels and copy number of pOXA-48 in wild type enterobacteria.** pOXA-
156 48 confers higher resistance levels and has a higher PCN in *Klebsiella* spp. than in *E. coli.* (A)
157 MIC (mg/L) of amoxicillin/clavulanic acid, ertapenem, imipenem and meropenem for the plasmid-
158 free/plasmid-carrying strain pairs (median of three biological replicates). (B) pOXA-48 plasmid

159 copy number (PCN) of the *E. coli* (n = 15) and *Klebsiella* spp. (n = 18) transconjugant strains.
160 PCN was estimated from sequencing data as the ratio of plasmid/chromosome median coverage
161 (see Methods). Horizontal lines inside boxes mark median values, the upper and lower hinges
162 correspond to the 25th and 75th percentiles, and whiskers extend to 1.5 times the interquartile
163 range. Dots indicate individual PCN values. To aid visualization, the y axis is represented in $\log_{10}$
164 scale with no value transformation. (C) pOXA-48 PCN in *E. coli* (n = 59) and *Klebsiella* spp. (n =
165 140) pOXA-48-carrying wild-type clinical strains. Boxplots are structured as in B. *$P < 0.05$, **P
166 < 0.01, ***$P < 0.001$.

167 **Conjugation frequency varies across clinical strains**

168 To analyze pOXA-48 horizontal transmission dynamics, we determined the ability of clinical
169 strains to acquire the plasmid by conjugation ("conjugation permissiveness"). For recipients, we
170 used a subset of 10 *Klebsiella spp.* and 10 *E. coli* strains representative of the genetic diversity
171 of the collection (Fig. S1). For donors, we used three pOXA-48-carrying strains. These were a
172 laboratory-adapted *E. coli* strain [β3914, a diaminopimelic acid (DAP) auxotrophic laboratory
173 mutant of *E. coli* K-12], and two wild-type pOXA-48-carrying clinical strains recovered from
174 hospitalized patients and belonging to STs responsible for between-patient plasmid dissemination
175 in the same hospital (28): *K. pneumoniae* ST11, and *E. coli* ST10 (strains K93 and C165
176 described in references 28 and 32).

177 We first performed classical conjugation assays (one donor and one recipient strain in equal
178 proportions) for all donor–recipient combinations, and measured conjugation frequencies as the
179 ratio between transconjugants (TC) and total recipient cells (see Methods for details). Note that
180 the donor *K. pneumoniae* ST11 could not be distinguished from three recipients of the same
181 species, either by the phenotype in the differential medium or by antibiotic selection, and therefore
182 conjugations could not be performed for these donor–recipient pairings. This analysis revealed a
183 wide diversity of conjugation frequencies across recipient strains. Overall, *Klebsiella spp.* strains
184 showed a significantly higher conjugation permissiveness than *E. coli* for all three donors (Fig.
185 2A, Kruskal-Wallis rank sum test: *E. coli* β3914, $X^2 = 45.8$, $P = 1.9 \times 10^{-11}$; *E. coli* ST10, $X^2 = 34.1$,
186 $P = 5.16 \times 10^{-9}$; *K. pneumoniae* ST11, $X^2 = 6.98$, $P = 8.24 \times 10^{-3}$). Moreover, three *E. coli* strains
187 produced no TCs with any of the donors, whereas all *Klebsiella spp.* strains produced TCs in at

188 least one of the conditions and were also the recipients with highest conjugation permissiveness
189 for every donor.

190 The gut microbiota is a dense bacterial community that engages in complex ecological
191 interactions. To analyze if community complexity could affect conjugation permissiveness in our
192 clinical strains, we repeated the conjugation assays, but this time instead of using a single clone
193 as the receptor, we used ten pairs of the *E. coli*/*Klebsiella* spp. strains (Fig. 2B and Table S1).
194 This analysis once again revealed great variability in reception frequencies and a higher overall
195 conjugation permissiveness in *Klebsiella* spp. strains (Fig. 2B, paired Wilcoxon signed-rank exact
196 test: *E. coli* β3914, $V = 235$, $P = 0.017$; *E. coli* ST10, $V = 205$, $P = 0.01$; *K. pneumoniae* ST11, V
197 $= 45$, $P = 1.2 \times 10^{-4}$). In general, the conjugation frequencies observed agreed with those from
198 the single conjugation assays, suggesting that ecological interactions did not markedly affect
199 conjugation dynamics. However, some of the *E. coli* strains that produced no TCs as single
200 receptors were able to acquire the plasmid, which could be due to secondary conjugations from
201 the *Klebsiella* spp. TC (33). Finally, to increase the complexity of the recipient community even
202 further, we performed conjugation assays using a pool of all 20 strains as recipients (Fig. 2C). In
203 this case, we could only distinguish between TCs at the species level in the differential medium.
204 Once again, the results revealed *Klebsiella spp.* to be more conjugation-permissive than *E. coli*,
205 regardless of the donor (Fig. 2C, Kruskal-Wallis rank sum test: *E. coli* β3914, $X^2 = 9.28$, $P = 2.32$
206 $\times 10^{-3}$; *E. coli* ST10, $X^2 = 9.31$, $P = 2.35 \times 10^{-3}$; *K. pneumoniae* ST11, $X^2 = 12.8$, $P = 3.49 \times 10^{-4}$).

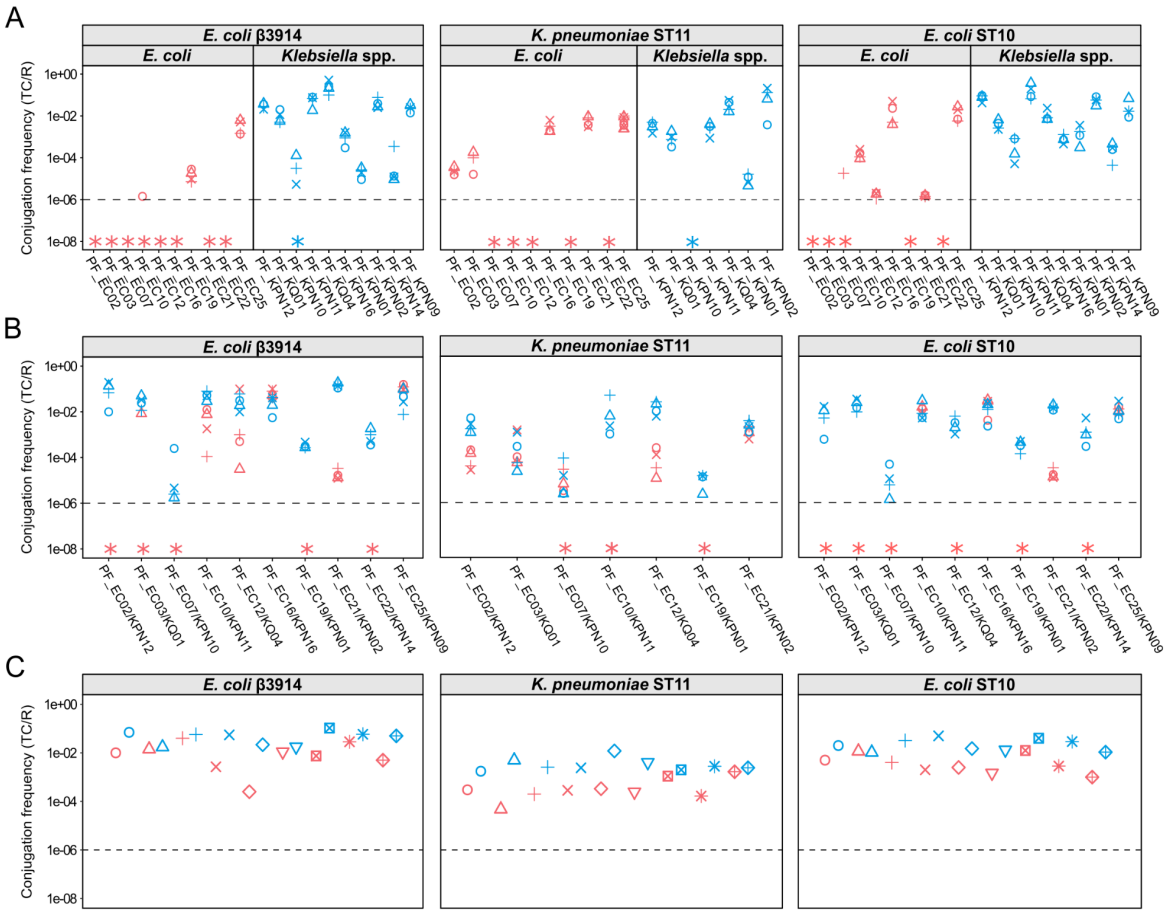

207

208 **Fig. 2. *In vitro* pOXA-48 conjugation dynamics in wild type enterobacteria**. Conjugation
209 frequencies (transconjugants/recipient) of a subset of 20 isolates from our clinical enterobacteria
210 collection (10 *E. coli* and 10 *Klebsiella* spp., x-axis), obtained from three pOXA-48 donors (*E. coli*
211 β3914, left; *K. pneumoniae* ST11, center; and *E. coli* ST10, right). (A) Conjugation frequencies
212 obtained in conjugation assays with one donor and one recipient in equal proportions. Color
213 represents the recipient species (red, *E. coli*; blue, *Klebsiella* spp.), symbols represent biological
214 replicates (n = 4), and asterisks symbolize conjugation frequencies below the detection limit
215 (dotted line). *Klebsiella spp.* exhibits higher conjugation frequencies than *E. coli* for the three
216 donors. (Kruskal-Wallis rank sum test: $P < 0.01$). (B) Conjugation frequencies using one donor
217 and pairs of *E. coli* and *Klebsiella* spp. as recipients. *Klebsiella spp.* is more conjugation-
218 permissive than *E. coli*, regardless of the donor used (Wilcoxon signed-rank exact test: $P < 0.02$).
219 (C) Conjugation frequencies obtained with a pool of recipients (one donor, 20 recipients). The
220 results give a conjugation frequency value per species, and symbols represent biological
221 replicates (n=9) whose values would correspond to the most successful strains of each species

222 in plasmid uptake. *Klebsiella spp.* has higher conjugation frequencies than *E. coli*, regardless of
223 the donor (Kruskal-Wallis rank sum test: $P < 0.01$).

224 **Conjugation dynamics in a mouse model of gut colonization**

225 To confirm our *in vitro* results in a more biologically relevant environment, we studied pOXA-48
226 conjugation dynamics in a mouse model of gut colonization (C57BL/6J). As donor, we used *K.*
227 *pneumoniae* ST11 strain K93, since this clonal group is frequently responsible for gut microbiota
228 colonization of patients in our hospital (28). As recipients, we used 6 strains representative of the
229 variability in conjugation frequency observed *in vitro* (*E. coli* PF_EC10, PF_EC12, and PF_EC21;
230 and *Klebsiella spp*. FP_KQ01, PF_KPN11, and PF_KPN12). Mice (n = 21) were treated orally
231 with ampicillin (0.5 g/L), vancomycin (0.5 g/L), and neomycin (1 g/L) for one week to reduce
232 colonization resistance, as we previously described (34), and the antibiotic treatment was stopped
233 one day before inoculation. A total of 18 mice were inoculated orally with the donor and co-
234 inoculated 2 hours later with the recipients (3 mice per recipient), and 3 mice were not inoculated
235 with any bacteria, as controls. Fresh fecal samples were collected every 24 hours during 2 days.
236 At the end of the second day, mice were sacrificed, and cecum samples were collected. Samples
237 were processed and plated with antibiotic selection to determine colonization levels and
238 conjugation frequencies, as described in Methods. Two independent assays were performed, two
239 months apart, and the results of both assays are compiled below (Fig. 3 and source data).

240 Colonization levels were high in all inoculated mice at both 24 and 48 hours for donor and recipient
241 strains (Fig. 3A), while no colonization was observed in the control mice. At 24 hours post-
242 inoculation, conjugation frequencies were generally low, and no differences in conjugation
243 frequencies were detected between *E. coli* and *Klebsiella* spp. (Fig. 3B Kruskal-Wallis rank sum
244 test H = 1.4, P = 0.265). At 48 hours post-inoculation, the levels of donors were similar in mice
245 co-inoculated with *E. coli* or *Klebsiella* spp. recipient strains (Wilcoxon rank sum test: in feces, W
246 = 2.71, P = 0.1; in cecum, W = 0.1, P = 0.752). However, despite the fact that the levels of
247 *Klebsiella spp.* recipients were slightly lower than those of *E. coli* recipients (Wilcoxon rank sum
248 test: in feces, W = 245, P = 0.008; in cecum, W = 4.9, P = 0.026), *Klebsiella spp.* showed
249 significantly higher conjugation frequencies (Fig. 3B, Kruskal-Wallis rank sum test: in feces, H =
250 24.6, $P = 6.89 \times 10^{-7}$; in cecum, $H = 10.2$, $P = 1.4 \times 10^{-3}$). In summary, the *in vivo* results correlated

251 qualitatively with those from the *in vitro* conjugation assays (Fig. 2A and 3B), and *Klebsiella spp.*
252 strains showed higher conjugation permissiveness than *E. coli* strains.

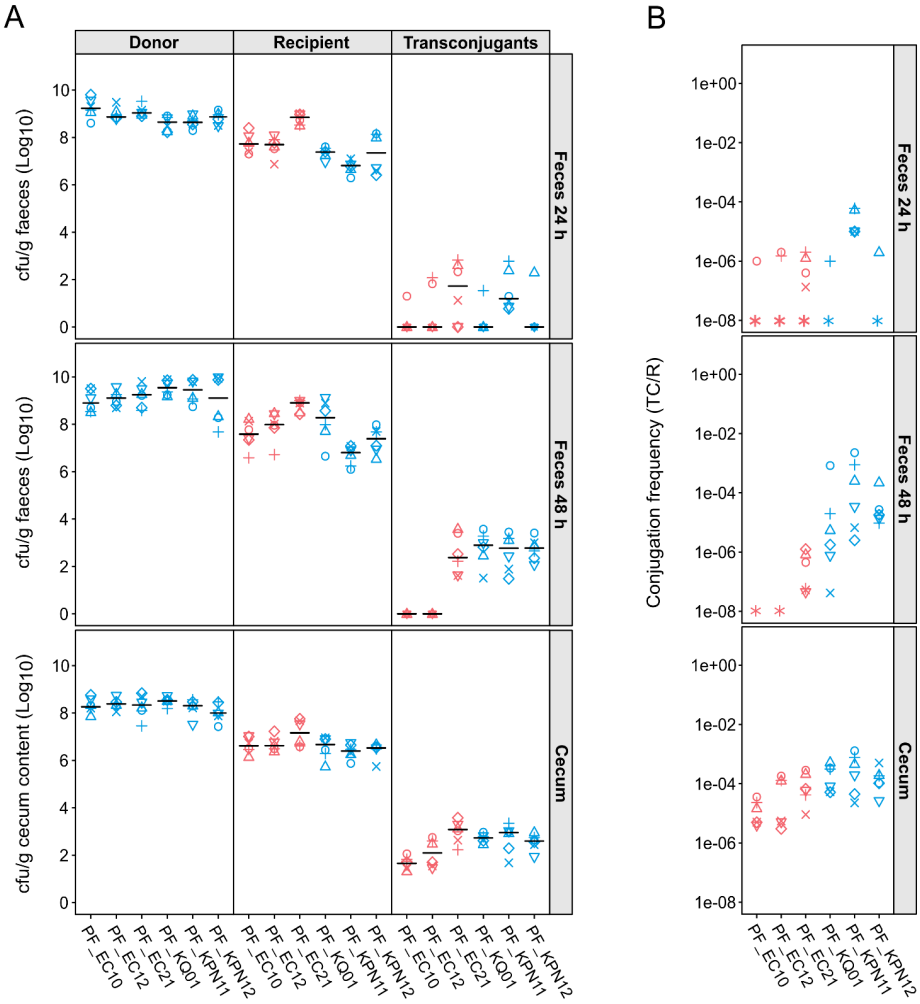

254 **Fig. 3. pOXA-48 conjugation dynamics in a mouse model of gut colonization**. pOXA-48
255 conjugation frequencies in mouse feces and cecum at 24 and 48 hours post colonization. (A)
256 Colonization levels in the donor (*K. pneumoniae* ST11), recipients (3 *E. coli* and 3 *Klebsiella spp.*
257 strains), and transconjugants, in feces at 24 and 48 hours post-inoculation (top and center) and
258 in cecum content at 48 h (bottom). Species are indicated by colors (red, *E. coli*; blue, *Klebsiella*
259 *spp.*) and biological replicates (n=6) by symbols. Black lines indicate the median values for the
260 biological replicates. Donor and recipient colonization levels were high in both feces and cecum.
261 (B) Conjugation frequencies (transconjugants/recipients) in feces at 24 and 48 hours (top and
262 center) and in cecum (bottom). Conjugation frequencies were significantly higher in *Klebsiella*
263 spp. than in *E. coli* in both feces and cecum at 48 hours (Kruskal-Wallis rank sum test in feces H
264 = 24.6, $P = 6.89 \times 10^{-7}$; in cecum H = 10.2, $P = 1.4 \times 10^{-3}$).

265 ***Klebsiella*-derived capsules are associated with plasmid carriage in *E. coli***

266 The conjugation experiments showed a higher permissiveness for pOXA-48 acquisition in
267 *Klebsiella* spp. than in *E. coli*, as well as high variability between strains of the same species. We
268 sought to investigate the genetic traits that could explain these differences. We analyzed the
269 genomes of the 20 recipient strains for an array of traits known to affect conjugation efficiency:
270 CRISPR arrays, restriction-modification (RM) systems and other phage defense systems that
271 could target pOXA-48, plasmid incompatibilities, and type VI secretion systems (T6SS, known to
272 mediate bacterial competition, which may affect conjugation frequencies). However, none of
273 these traits accounted for the observed differences in pOXA-48 acquisition (Fig. S4, Table S2).

274 Capsules have been reported to hinder DNA transfer and possibly constitute a barrier to plasmid
275 acquisition (35). We used two software tools to search for capsular systems: Kaptive, to detect
276 and type *Klebsiella* capsular loci, and CapsuleFinder, to identify other capsular systems. With the
277 single exception of the non-capsulated PF_KPN14 strain, each recipient strain encoded a specific
278 set or type of complete capsular loci (Table S2). To assess whether similar sets of capsular loci
279 were associated with higher or lower conjugation permissiveness, we calculated a weighted gene
280 repertoire relatedness (wGRR) score. Although we found no clear pattern for the *Klebsiella* spp.
281 recipients, the *E. coli* strain with the highest pOXA-48 reception rate, PF_EC25, encoded a
282 *Klebsiella* capsular locus (KL35, Fig. 4A, Table S2).

283 To determine if *Klebsiella*-derived capsules better facilitate pOXA-48 acquisition than other
284 capsular systems, we analyzed their association in the complete genomes of 1,585 *E. coli* and
285 715 *K. pneumoniae* strains (RefSeq), of which 6 *E. coli* strains and 46 *K. pneumoniae* strains
286 carry pOXA-48 (Fig. 4B, Table S3). We used phylogenetic logistic regression (*phyloglm*) to
287 account for phylogenetic dependency of the significant associations ($P < 0.05$, Fisher's exact test;
288 Table S5). The presence of *Klebsiella*-derived capsules was associated with pOXA-48 carriage
289 only when *E. coli* and *K. pneumoniae* were analyzed together (Table S5, *phyloglm* $P = 0.0016$).
290 We next investigated the relationship between the presence of *Klebsiella*-derived capsules and
291 plasmid carriage more generally, finding significant associations when analyzing *E. coli* and *K.*
292 *pneumoniae* together (Table S5, *phyloglm* $P < 2 \times 10^{-16}$) and when analyzing *E. coli* separately
293 (Table S5, *phyloglm* $P = 2.2 \times 10^{-5}$). Moreover, *E. coli* strains encoding other capsular systems
294 (not derived from *Klebsiella*) were more likely to be plasmid-free or to carry only one plasmid,

295 whereas *E. coli* encoding *Klebsiella*-derived capsules had an increased likelihood of carrying
296 multiple plasmids (Fig. 4C). These results suggest that although capsules generally obstruct
297 conjugation (35), certain types of *Klebsiella*-derived capsules could be more permissive than
298 other capsule types to plasmid acquisition by *E. coli*.

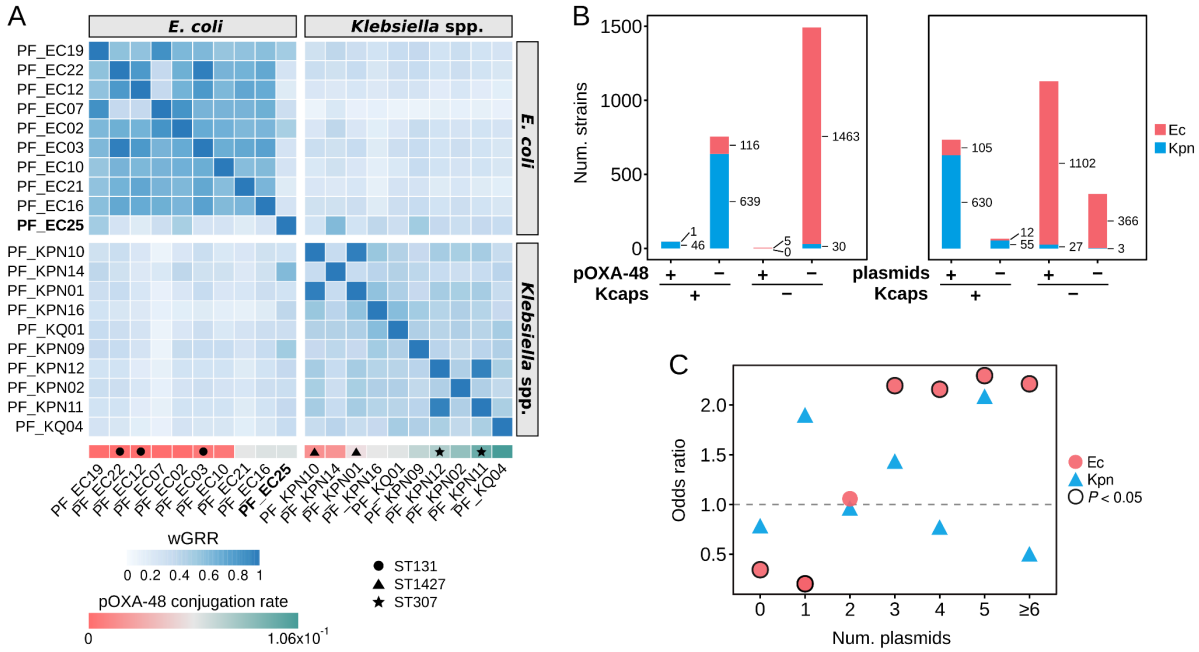

299

300 **Fig. 4. Associations between capsular systems and plasmid carriage**. Analysis of capsular
301 systems and plasmid prevalence in our recipient strains and in *E. coli* and *K. pneumoniae*
302 genomes obtained from RefSeq. (A) Heatmap of weighted gene repertoire relatedness (wGRR)
303 scores between capsular sets (*Klebsiella*-derived capsules and/or other capsular systems)
304 encoded by the recipient strains used in conjugation experiments. A wGRR score of 1 means that
305 all proteins from the capsular set encoding the fewest number of proteins have a homolog in the
306 capsular set it is compared with. A score of 0 indicates there are no homologs between the
307 capsular sets of the two compared strains. Recipients are ordered by mean pOXA-48 conjugation
308 frequency across replicates and experimental conditions. The PF_EC25 strain, highlighted in
309 bold, has the highest mean conjugation frequency of any *E. coli* strain and is the only *E. coli* strain
310 encoding a *Klebsiella*-derived capsule. Strains from the same sequence type (ST) are marked
311 with a symbol. (B) Number of *E. coli* (Ec) and *K. pneumoniae* (Kpn) strains from the RefSeq
312 database analyzed for the association between the presence of *Klebsiella*-derived capsules
313 (Kcaps) and carriage of pOXA-48 (left) or plasmids in general (including pOXA-48; right). In total,
314 the RefSeq database includes 1,585 Ec and 715 Kpn strains. (C) Association between the

315 presence of a genome-encoded *Klebsiella*-derived capsule and the number of plasmids carried
316 in the *E. coli* (Ec) and *K. pneumoniae* (Kpn) RefSeq strains. The chart shows odds ratio (Fisher's
317 exact test) of plasmid carriage for strains encoding a *Klebsiella*-derived capsule *vs* strains
318 encoding other capsular systems (not from *Klebsiella*). Values above 1 (horizontal dashed line)
319 indicate a positive association, and values below 1 a negative association, between encoding
320 *Klebsiella*-derived capsules and carrying the indicated number of plasmids. In all cases, the
321 number of strains carrying each number of plasmids is >100. A significant Fisher's test ($P < 0.05$)
322 is indicated by a black outline.

323 **Modeling the impact of vertical and horizontal transmission dynamics on plasmid**
324 **distribution.**

325 We previously developed a mathematical model to study how pOXA-48 fitness effects impact
326 plasmid maintenance in complex bacterial communities (32). That model allowed us to predict
327 the competitive fitness of each strain, with and without pOXA-48, based on growth-kinetic
328 parameters that were calibrated from experimental growth curves obtained from single clones
329 (Methods). In the present study, we extended this model to include the new variables informed
330 by the experimental results: conjugation permissiveness and resistance levels (Fig. 5A). We used
331 this extended model to numerically simulate different enterobacteria community compositions and
332 environmental regimes, with the aim of estimating the stability of different plasmid-host
333 associations. This computational model allowed us to track the distribution of plasmids in
334 response to fluctuating selection at strain and species resolution.

335 We first simulated pairwise competition experiments between the 10 *Klebsiella* spp. and 10 *E.*
336 *coli* strains in our collection with experimentally determined conjugation frequencies and AMR
337 levels. Each competition experiment started with a 1:1 ratio, and a 50% plasmid frequency in each
338 strain (Methods). The total of 1,000 stochastic simulations were performed in environments with
339 daily changes in drug concentration determined by a Gaussian signal noise, with a probability
340 density function equal to that of the normal distribution (Fig. S5). In these simulations, most
341 pairwise associations were able to maintain the plasmid in the absence of selection, with similar
342 probabilities of finding the plasmid in an *E. coli* strain (35%) or in a *Klebsiella* spp. strain (38%)
343 (Fig. S6-S7). To assess the role of antibiotics in the distribution of plasmids in the population, we

344 increased the maximal drug concentration in the environment and repeated all pairwise
345 competition experiments for a range of selection pressures (Fig. S6). The fraction of pairwise
346 associations that rendered the plasmid stable peaked at intermediate selection strength (Fig. S7).
347 Notably, due to the lower resistance levels exhibited by *E. coli* strains, the frequency of *Klebsiella*
348 spp. strains in the population increased in direct correlation with the selection strength.

349 We next used the model to reproduce the population dynamics of pOXA-48 in the gut microbiota
350 of hospitalized patients, in order to analyze the impact of vertical and horizontal transfer dynamics
351 in plasmid distribution. Our previous epidemiological studies revealed that patients are commonly
352 colonized by pOXA-48-carrying nosocomial enterobacterial clones (30). During colonization, the
353 plasmid can spread horizontally to resident enterobacteria in the gut community, and different
354 clones can subsequently maintain the plasmid in the community, producing long term pOXA-48
355 gut carriage (30). To reproduce plasmid invasion and dissemination in the gut microbiota
356 community, we used the mathematical model to perform a multistrain computer simulation in
357 which only one member of the community carried pOXA-48 at the onset of the simulation (starting
358 at 0.1% frequency in the community; Fig. S8). Similar to the pairwise comparison, computer
359 simulations of polymicrobial communities also resulted in a reduction in the frequency of *E. coli*
360 strains as the drug concentration increased (Fig. 5B). Simulation of the ecological dynamics of
361 bacterial communities of increasing complexity (increasing number of individuals) revealed that,
362 in drug-free environments, pOXA-48 was found both in *E. coli* and *Klebsiella* spp. strains
363 independently of the number of strains in the community (Fig. 5C). In contrast, in the presence of
364 antibiotics, not only was the plasmid present mostly in highly-resistant *Klebsiella* spp. strains but,
365 as the number of strains in the community increased, so did the relative abundance of pOXA-48-
366 carrying *Klebsiella* spp. strains (Fig. 5D).

367 To explore the theoretical distribution of pOXA-48 among the different strains in a community, we
368 retrospectively analyzed parameter values of strains in which the plasmid remained stable during
369 stochastic simulations. In no-drug environments, simulations indicated the presence of pOXA-48
370 in strains with high growth rates, characterized by high cell efficiency and specific affinity (Fig.
371 5E,G). In contrast, in the presence of antibiotics, pOXA-48 was mostly found in highly resistant
372 strains (Fig. 5F,H). Notably, specific strains in the community played a significant role in stabilizing
373 the plasmid within the population; in our numerical simulations, the plasmid remained stable in

374 the population when, for example, strains PF_KQ04 or PF_EC16 were present, independently of
375 the selection strength and the fitness effects pOXA-48 produced in other members of the
376 community (Fig. S9). These strains were both highly resistant and highly plasmid permissive,
377 suggesting that successful plasmid-host associations in the microbiota are critical determinants
378 of plasmid invasion in complex microbial communities.

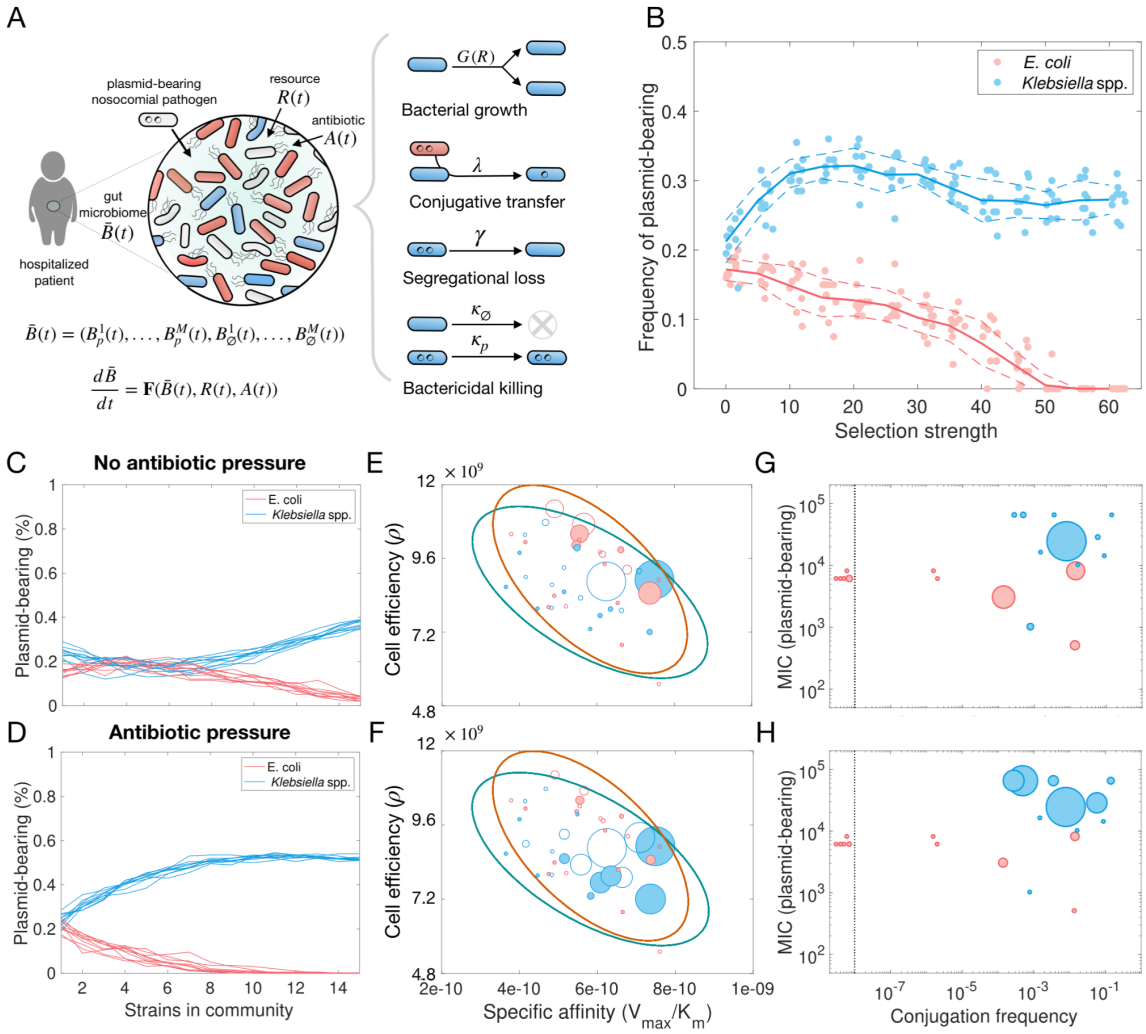

379

380 *Fig. 5*: **Theoretical modeling results.** (A) Scheme of the theoretical model used to simulate
381 plasmid invasion of a polymicrobial community composed of M strains. Plasmid dynamics are
382 driven by the rates of conjugative transfer (γ) and segregational loss (λ), as well as by the degree
383 of resistance (κ) and growth rate ($G(R)$), in environments with a limiting resource ($R(t)$) and a
384 bactericidal antibiotic ($A(t)$). (B) Frequency of plasmid-bearing *E. coli* strains (red) and a
385 *Klebsiella* spp. strains (blue) as a function of the maximum selection strength imposed by the
386 environment (A_{max}). As selection for the plasmid increases, the frequency of plasmid-carrying *E.*

387 *coli* strains is reduced, whereas the frequency of *Klebsiella* spp. strains remains constant. (C-D)
388 Frequency of plasmid-bearing strains as a function of the number of individuals in the community.
389 Each numerical experiment was performed for 100 random communities exposed to 10 different
390 stochastic environments, with increasing selective pressures. Top panel shows drug free
391 environments, $A_{max} = 0$, and bottom panel illustrates intermediate selective pressures, $A_{max} =$
392 0.1. In all cases, increasing the complexity of the population increases the likelihood of the plasmid
393 finding a successful association with a *Klebsiella* spp. strain. This effect is particularly pronounced
394 as the strength of selection increases. (E-F) Bidimensional representation of growth kinetic
395 parameters. *E. coli* strains are represented in red and *Klebsiella* spp. strains in blue ($A_{max} = 0$;
396 panel E, $A_{max} = 0.1$; panel F). Empty circles represent plasmid-free strains and solid circles
397 represent plasmid-carrying strains. The diameter of each circle is proportional to the number of
398 times each strain was detected at the end of a numerical experiment. Ellipses illustrate standard
399 deviations of best-fit normal distributions (plasmid-bearing strains in green and plasmid-free cells
400 in orange). (G-H) Plots illustrating conjugation permissiveness (TC/recipients) and level of AMR
401 (MIC in mg/L) of each plasmid-carrying strain. Vertical dotted line in the conjugation frequency
402 axis illustrates the detection limit. In the absence of selection ($A_{max} = 0$; panel G), both *Klebsiella*
403 spp. and *E. coli* strains with a high specific affinity and cell efficiency were frequently detected. In
404 the presence of positive selection for the plasmid ($A_{max} = 0.1$; panel H), almost exclusively
405 *Klebsiella* spp. strains with high levels of resistance survive. These findings suggest that antibiotic
406 selection plays a crucial role in shaping plasmid distribution in clinical enterobacteria.

407 **Discussion**

408 In this study, we performed a comprehensive analysis of the vertical and horizontal transmission
409 dynamics of the carbapenem resistance plasmid pOXA-48 in clinical enterobacteria. An important
410 conclusion of our study is that these dynamics are far from being constant across different wild
411 type bacterial hosts. We had previously shown that pOXA-48 produces variable fitness effects in
412 the absence of antibiotics (30), and in this new study we reveal similar variability in traits important
413 for vertical transmission in the presence of antibiotics (AMR levels, Fig. 1), and horizontal
414 transmission (conjugation, Figs. 2 and 3). This variability is especially evident for horizontal
415 transmission, with conjugation frequencies differing by orders of magnitude across different
416 recipients. Despite this variability, our results indicate that, compared with *E. coli*, *Klebsiella* spp.

417 clones generally have a higher AMR level associated with pOXA-48 carriage and a greater ability
418 to take up pOXA-48 by conjugation. These results may help to explain why pOXA-48 is usually
419 associated with *K. pneumoniae* clones in clinical settings (28, 29).

420 A key advantage of experimentally determining plasmid-associated traits in a collection of wild
421 type clinical enterobacteria is that we can confidently feed these variables into mathematical
422 models in order to ask general questions about pOXA-48 dynamics in complex bacterial
423 communities. In this study, we developed a model including three key variables informed by our
424 experimental results: bacterial growth dynamics with and without pOXA-48, conjugation
425 permissiveness, and AMR levels. We used this model to investigate plasmid dynamics under
426 different fluctuating regimes of selection pressure and community complexity, aiming to simulate
427 pOXA-48 invasion of a gut microbiota (Fig. 5). Our results reveal that vertical transmission is
428 probably the most critical factor modulating the distribution of plasmids in polymicrobial
429 communities. Specifically, in the absence of antibiotics, the growth dynamics of plasmid-carrying
430 clones determine which strains maintain the plasmid (Fig. 5E), whereas in the presence of
431 antibiotics, plasmid distribution is primarily determined by AMR level (Fig 5H). However, as
432 expected, horizontal transmission also plays a significant role in plasmid distribution in
433 communities, and strains showing low-to-zero conjugation permissiveness very rarely maintain
434 pOXA-48 (conjugation frequency < 10^{-4}, Fig. 5G,H).

435 Arguably the most important result of our simulations is that a single successful pOXA-48-
436 bacterium association is sufficient to allow for plasmid invasion and stable maintenance in a
437 complex population, regardless of plasmid effects on the remaining community members. These
438 jackpot associations, combining high growth rates, high AMR levels, and high conjugation
439 permissiveness, can act as pOXA-48 super-sinks in the gut microbiota of patients, maintaining
440 and further disseminating the plasmid. More generally, our results indicate that plasmid
441 transmission dynamics can help predict successful associations between high-risk bacterial
442 clones and AMR plasmids of epidemiological relevance. For example, we showed that the two *K.*
443 *quasipneumoniae* strains tested in this study (PF_KQ01 and PF_KQ04) produced successful
444 associations with pOXA-48 (Fig. S9), suggesting that this species, which has been previously
445 associated with pOXA-48 in our hospitals and others (28, 29 36-38), may play an important role
446 in pOXA-48 epidemiology. Our results could also have implications for the design of interventions

447 aimed at reducing the spread of antibiotic resistance. For example, new strategies that specifically
448 target these successful associations, using biotechnological tools such as those based on
449 CRISPR or toxin-inteins (39, 40), would dramatically increase our ability to control AMR
450 dissemination in clinical settings.

451 Given the importance of vertical and horizontal plasmid transmission in the evolution of plasmid-
452 mediated AMR, a critical research direction in the field will be to characterize the molecular basis
453 of the observed high variability in transmission-associated traits. Understanding the plasmid and
454 host factors that determine this variability will help us not only to predict, but also hopefully to
455 counteract successful associations between AMR plasmids and high-risk bacterial clones. In this
456 study, we showed that the presence of *Klebsiella*-derived capsules, compared to other capsular
457 systems, is associated with a higher plasmid frequency in *E. coli* clones (Figure 4) and that pOXA-
458 48 PCN is higher in *Klebsiella* spp. than in *E. coli* clones (Figure 1). Further work will be needed
459 to characterize the molecular basis and significance of these and other specific interactions.

460 **Methods**

461 **pOXA-48_K8 plasmid, strains, and growth conditions.** To analyze the pOXA-48-associated
462 AMR level, we selected 33 isogenic strains pairs (15 *E. coli* and 18 *Klebsiella* spp.) with (TC) or
463 without pOXA-48 plasmid (PF) from our collection of ecologically compatible enterobacterial
464 isolates from the human gut microbiota (Table S1, partially overlapping the collection in (30)).
465 Plasmid-bearing strains carry the most common pOXA-48-like plasmid variant from our hospital,
466 pOXA-48_K8 (26). For the conjugation frequencies determination, we selected, as recipients, 10
467 *E. coli* and 10 *Klebsiella spp.* pOXA-48-free isolates that cover the phylogenetic diversity of the
468 collection (Fig. S1) (30) and showed similar β-lactam resistance levels. As plasmid donors we
469 selected three pOXA-48_K8-carrying strains: *E. coli* β3914 (30, 40), *K. pneumoniae* K93 (32) and
470 *E. coli* C165 (32). Bacterial strains were cultured in LB at 37 °C with continuous shaking (250
471 r.p.m), and on LB or HiCrome^{TM} UTI (Himedia Laboratories, India) agar plates at 37 °C.

472 **Determination of minimum inhibitory concentration (MIC).** We determined the MIC of AMC
473 (Normon, Spain), ERT (Merck Sharp & Dohme B.V., Netherlands), IMP (Fresenius Kabi,
474 Germany) and MER (SunPharma, India) in all plasmid-carrying and plasmid-free clones selected
475 for this study following a modified version of the agar dilution protocol (42, 43). This method allows

476 us to test a large number of isolates simultaneously under identical conditions and to test a wide
477 range of AMC concentrations, since this β-lactam antibiotic degrades fast in liquid medium (44).
478 We prepared pre-cultures of plasmid-free and plasmid-carrying strains by inoculating single
479 independent colonies into LB broth in 96-well plates and overnight incubation at 37 ºC with
480 continuous shaking (250 r.p.m.). We spotted 10 µl of each overnight culture onto LB agar plates
481 with increasing concentrations of AMC (from 4 mg/L to 32,768 mg/L), ERT (from 0,25 mg/L to 512
482 mg/L), IMP (from 0.25 mg/L to 1,024 mg/L) or MER (from 0.25 mg/L to 32 mg/L), and incubated
483 them overnight at 37 ºC. We determined the MIC of each strain as the lower antimicrobial
484 concentration able to inhibit the growth of each strain. We performed three biological replicates
485 per MIC determination in three independent days, and we used the median value of the three
486 replicates as the MIC.

487 ***In vitro* determination of conjugation frequencies.** To determine the *in vitro* conjugation
488 frequencies, we selected, as recipient strains, 10 *E. coli* and 10 *Klebsiella spp.* pOXA-48-free
489 isolates, from our collection of ecologically compatible enterobacterial isolates (Fig. S1). As
490 plasmid donors we used three pOXA-48_K8-carrying strains: *E. coli* β3914, a counter-selectable
491 diaminopimelic acid auxotrophic laboratory strain (30); *K. pneumoniae* K93 (322), a pOXA-48-
492 carrying ST11 strain; and *E. coli* C165 (32), a pOXA-48-carrying ST10 strain. To counter-select
493 the two natural donors, we transformed the recipients with pBGC plasmid, a non-mobilizable *gfp*-
494 carrying small plasmid that encodes a chloramphenicol resistance gene (30). It was not possible
495 to introduce pBGC into three *Klebsiella spp.* isolates (PF_KPN09, PF_KPN14 y PF_KPN16), due
496 to their level of constitutive resistance to chloramphenicol. We streaked donor and recipient
497 strains from freezer stocks onto LB agar plates with or without ertapenem 0.5 mg/L –and 0.3 mM
498 DAP for *E. coli* β3914/pOXA-48_K8–, respectively, and incubated at 37 °C overnight. We
499 prepared pre-cultures of donors and recipients by inoculating single independent colonies in 15-
500 ml culture tubes containing 2 ml of LB broth and overnight incubation at 37 ºC with continuous
501 shaking (250 r.p.m.). To perform classic conjugation assays, we mixed one donor and one
502 recipient at equal proportions (each donor with each recipient, independently, with a total of 4
503 recipient biological replicates by donor), plated the mixture as a drop onto LB agar plates –
504 supplemented with DAP 0.3mM for *E. coli* β3914/pOXA-48_K8 donor– and incubated them at 37
505 ºC during only 4h (to avoid secondary conjugation events and the impact of potential differences

506 in donor, recipient, and transconjugant growth rates on conjugation frequency determination).
507 After incubation, we collected the biomass, resuspended it in 1 ml of NaCl 0.9 % and performed
508 1/10 serial dilutions up to 10^{-6}. We estimated the final densities of transconjugants and recipients
509 by plating 10 µl of each dilution on HiCrome™ UTI agar plates (HIMEDIA laboratories, India) with
510 or without AMC 256 mg/L, respectively, and with chloramphenicol 50 mg/L. We plated the
511 dilutions as drops, and each drop was subsequently allowed to drain down the plate, this way we
512 can separate the colonies so they are easily distinguishable and quantifiable. We performed the
513 donor counter-selection by the absence of DAP in the medium for *E. coli* β3914/pOXA-48_K8, or
514 by selection with chloramphenicol for clinical *K. pneumoniae* ST11 and *E. coli* ST10. Finally, we
515 calculated the conjugation frequencies per recipient following the formula below:

516 $$Conjugation\ frequency_R = \frac{CFU_{transconjugants}}{CFU_{recipient}}$$

517 where $CFU_{transconjugants}$ are the transconjugant colony-forming units obtained from the number of
518 colonies in the plate (corrected by the dilution factor); and $CFU_{recipient}$ are the number of recipient
519 colony-forming units minus transconjugants. Note that in the cases where no TC colonies were
520 detected in the plate, we calculated a threshold conjugation frequency assuming the presence of
521 a single colony in the total cell suspension, thus establishing a detection limit of 10^{-6}.

522 To perform conjugation assays with recipient pairs we randomly grouped the recipients in pairs
523 so that each pair comprised one *E. coli* and one *Klebsiella spp.* recipient. We used a modified
524 version of the above protocol, in which we mixed recipient pre-cultures of each pair at equal
525 proportions and we subsequently mixed these recipient mixtures with the pre-culture of the donor
526 at the same proportion, forming the final conjugation reaction (each recipient pair with one donor
527 per time, with 4 biological replicates of recipient pairs). We determined the recipients and
528 transconjugants densities by antibiotic selection with AMC 256 mg/L, (to select transconjugants
529 vs. recipients) and chloramphenicol 50 mg/L (to counter-select donors), and distinguished
530 between recipients using the differential chromogenic medium HiCrome™ UTI agar. We
531 calculated the conjugation frequency per each receptor using the formula above.

532 For conjugation assays with a pool of all the recipients, we mixed the same pre-culture volume of
533 all recipient strains with one donor per experiment, following the same protocol previously
534 described. Nine biological replicates were performed.

535 ***In vivo* determination of conjugation frequencies.** For the determination of conjugation
536 frequencies of clinical isolates *in vivo*, we performed conjugation assays using a mouse model of
537 gut colonization. We selected a subset of 6 pBGC-carrying (30) recipient strains from the *in vitro*
538 conjugation assays: 3 *E. coli* (PF_EC10, PF_EC12 and PF_EC21) and 3 *Klebsiella spp.*
539 (PF_KQ01, PF_KPN11 and PF_KPN12) strains. As plasmid donor we selected the natural pOXA-
540 48_K8-carrying isolate, *K. pneumoniae* ST11, K93 (32). We carried out the experiment described
541 below twice, 2 months apart and under identical conditions.

542 *Mouse model and housing conditions*. We used 6-week-old C57BL/6J female mice (n =
543 21) purchased from Charles River Laboratories and housed them with autoclave-sterilized food
544 (a 1:1 mixture of 2014S Teklad Global diet and 2019S Teklad Global Extrused 19% Protein
545 Rodent Diet from Envigo) and autoclave-sterilized water. Temperature was kept at 21 ± 2 °C and
546 humidity was maintained at 60–70%, in 12 h light/dark cycles. To allow intestinal colonization of
547 the donor and recipient strains, we disrupted the intestinal microbiota by administering ampicillin
548 (500 mg/L), vancomycin (500 mg/L) and neomycin (1 g/L) in the drinking water for one week, as
549 previously described (34). Water with antibiotics was changed every 3-4 days to avoid reduction
550 of antibiotic activity. During antibiotic treatment, mice were co-housed (3-6 mice per cage). After
551 1 week of treatment, antibiotics were removed from the drinking water and mice were individually
552 housed to avoid bacterial transfer between mice due to coprophagia during the experiment.

553 *Mice inoculation with donor and recipient strains.* 1 day after antibiotic treatment removal,
554 18 out of 21 mice were inoculated by oral gavage with 10^7 CFU of the donor strain, *K. pneumoniae*
555 ST11. Two hours later, each donor-inoculated mouse was co-inoculated by oral gavage with 10^7
556 CFU of a recipient strain (3 mice per recipient). This way, from the initial 21 mice, 18 of them were
557 inoculated with donor and recipient bacteria (6 different recipients, 3 mice per recipient) and 3
558 mice remained uninoculated as control.

559 *Sample collection and bacterial levels determination.* After antibiotic treatment and prior
560 to inoculation, we collected fresh fecal samples from each mouse as to control for the absence of
561 bacteria able to grow on the selective medium used for our bacteria of interest. We weighted the
562 feces and resuspended them in 1 ml PBS until a homogeneous mixture was obtained. Then, we
563 diluted mixtures 1:100,000 and plated 100 µl on HiCrome$_{TM}$ UTI agar plates with ampicillin (400
564 mg/L) and vancomycin (1 mg/L). We incubated the plates overnight at 37 ºC. After incubation,

565 bacterial growth was found to be absent. During the assay, we collected fresh fecal samples from
566 each mouse 24 and 48 h post inoculation and processed samples as described before. To
567 determine the donor, recipients and transconjugants densities, we plated 100 µl of different
568 dilutions onto HiCrome™ UTI agar plates with: i) vancomycin (1 mg/L) and AMC (256 mg/L) to
569 detect the donor; ii) vancomycin (1 mg/L) and chloramphenicol (50 mg/L) to detect recipients; and
570 iii) vancomycin (1 mg/L), AMC (256 mg/L) and chloramphenicol (50 mg/L) to determine the
571 presence of transconjugants. We calculated the colonization levels of the members of each
572 conjugation assay with the following formula:

573 $$UFC/mg_{donor,recipient} = \frac{UFC_{donor,recipient} - UFC_{transconjugants}}{mg_{feces}}$$

574 From the levels of recipients and transconjugants we calculated the conjugation frequencies per
575 recipient as described before in the *in vitro* protocol. At 48 h post inoculation, after fresh fecal
576 samples collection, we sacrificed mice and obtained samples of cecum content by manual
577 extrusion. We performed sample processing, bacterial levels determination and conjugation
578 frequencies determination as described above.

579 **DNA extraction and genome sequencing.** We isolated the genomic DNA of the strains used in
580 this work using the Wizard genomic DNA purification kit (Promega, WI, USA) and quantified using
581 the Qubit 4 fluorometer (ThermoFisher Scientific, MA, USA). Whole genome sequencing was
582 performed at the Wellcome Trust Centre for Human Genetics (Oxford, UK) using the Illumina
583 HiSeq4000 or NovaSeq6000 platforms with 125 or 150 base pair (bp) paired-end reads,
584 respectively. Read data is available under the BioProject PRJNA803387.

585 **Processing of sequencing data.** All Illumina reads were trimmed with a quality threshold of 20
586 and reads shorter than 50 bp and adapters were removed using Trim Galore v0.6.6
587 (https://github.com/FelixKrueger/TrimGalore). PF and TC genomes were *de novo* assembled with
588 SPAdes v3.15.2 (45) in --isolate mode and with the --cov-cutoff flag set to auto. Assembly quality
589 was assessed with QUAST v5.0.2 (46). TC were confirmed to correspond to their PF strain by
590 checking mutations and plasmid content with Snippy v4.6.0 (https://github.com/tseemann/snippy)
591 and ABRicate v1.0.1 (PlasmidFinder database, https://github.com/tseemann/abricate),
592 respectively. Snippy was also used to confirm isogenicity of the acquired pOXA-48 plasmids.

593 Multilocus sequence typing was performed with MLST v2.21.0
594 (https://github.com/tseemann/mlst).

595 **Construction of phylogenetic trees.** Mash distance phylogenies were constructed for the 25 *E.*
596 *coli* and 25 *Klebsiella* spp. PF strains from their whole-genome assemblies using mashtree v1.2.0
597 (47) with a bootstrap of 100 (Fig. S1).

598 **Plasmid copy number (PCN) estimation.** PCN of pOXA-48 was determined for the 33 TC
599 strains and the 200 wild-type *E. coli* and *Klebsiella* spp. R-GNOSIS strains (BioProject
600 PRJNA626430) carrying pOXA-48 variants sharing 72% of the pOXA-48_K8 core genome (32).
601 PCN was estimated from read coverage data as the ratio of plasmid median coverage by
602 chromosome median coverage (45, 46). Since the genome assemblies are fragmented, the
603 median coverage of the chromosome was calculated from the first three, largest contigs (total
604 size sum of first three contigs 0.3-4.0 Mb), which were confirmed to correspond to chromosomal
605 sequences by using BLASTn against the NCBI nr nucleotide database. The median coverage of
606 pOXA-48 was calculated from the contig containing the IncL replicon, as identified with ABRicate
607 v1.0.1 with the PlasmidFinder database, which generally corresponds to the largest pOXA-48
608 contig (size 11.0-59.8 Kb). For computing the PCN, the Illumina trimmed reads were first mapped
609 to their respective genome assembly using BWA MEM v0.7.17 (50). Strain K25 from the wild-type
610 pOXA-48-carrying collection was removed from the analysis due to truncated reads. Samtools
611 depth v1.12 (51) with the -a flag was used to obtain read depths at each genomic position and
612 the median read coverage for pOXA-48 and chromosome was computed with GNU datamash
613 v1.4 (gnu.org/software/datamash).

614 **Comparative genomic analysis of recipient strains.** We analyzed the genomes of the recipient
615 strains to find traits that could explain the observed differences in pOXA-48 acquisition. First, the
616 draft genomes of the 20 recipients and three donors (*E. coli* ST10 C165 and *K. pneumoniae* ST11
617 K93 from Bioproject PRJNA626430; for *E. coli* β3914, the sequence of the ancestral K-12 strain,
618 NC_000913.3) were annotated with Prokka v1.14.6 (52) with default settings. A summary of the
619 results can be found in Table S2.

620 Restriction-modification (RM) systems were searched using two approaches. First, the protein
621 sequences of the recipient and donor strains were blasted against the protein "gold standard"

622 REBASE database (downloaded February 2022, (53)) using BLASTp v2.9.0 (54). The results
623 were filtered with a criteria based on (55). Briefly, hits with type I and IIG RM systems were kept
624 if the percentage of identity and alignment was 100%, since it was observed that recognition sites
625 varied between enzymes with only a few mismatches. For type II systems, a threshold of 70%
626 identity and 90% alignment was used, as it was previously reported that these systems with
627 identity over 55% generally share the same target motifs. For type III and type IV this threshold
628 was higher, as reported in the same study, and was set at 90% identity and 90% alignment. After
629 filtering, some proteins had hits with more than one enzyme. For these cases, the best hit or the
630 hit with the enzyme of the corresponding organism (*E. coli* or *Klebsiella* spp.) was kept. The
631 DefenseFinder webserver (accessed February 2022, (56, 57)) was also used to search for RM
632 systems in the proteomes of recipients and donors. Then, the REBASE hits and the RM systems
633 detected by DefenseFinder were unified by protein ID. Enzymes or RM systems present in all
634 strains were discarded, since they would not explain differences in conjugation frequencies
635 between isolates. Finally, only complete RM systems that were not present in the donor strains
636 were retained for each recipient-donor combination, since the donor would be conferring
637 protection to pOXA-48 against equivalent systems of the recipient. Complete type I systems
638 comprise a restriction enzyme (REase), a methylase (MTase) and a specificity (S) subunit. Type
639 II systems include at least a REase and a MTase. No type III systems were detected, and type IV
640 systems are normally composed of one or two proteins. Donor and recipient systems were
641 regarded as similar if they shared the same recognition sequence or if a BLASTp alignment of
642 the enzymes followed the previous criteria of identity and alignment percentage per type of
643 system. The same method was applied for comparing the final systems between recipient strains,
644 and similar systems within each type were given the same letter code identifying the RM system
645 subtype (Fig. S4, Table S2).

646 Clustered regularly interspaced short palindromic repeats (CRISPRs) were identified in the
647 nucleotide sequences of the recipient strains with the DefenseFinder webserver. The spacer
648 sequences were aligned to pOXA-48_K8 (MT441554) using the blastn-short function of BLASTn
649 v2.9.0 (54) and hits were then filtered by percentage of alignment. Other defense systems were
650 also detected with the DefenseFinder webserver and PADLOC v1.1.0 (database v1.3.0, (58)).

651 Plasmid incompatibility was investigated by identifying plasmid replicons using ABRicate v1.0.1
652 with the PlasmidFinder database.

653 Secretion systems were searched using the TXSScan models of MacSyFinder v1.0.5 (56, 59),
654 selecting the option "ordered_replicon" and linear topology. Only complete systems were
655 considered.

656 Capsular systems were identified using two software. First, *Klebsiella* capsules, which belong to
657 the Wzx/Wzy-dependent group I capsular systems, were identified with Kaptive v2.0.0 (60), using
658 the K locus primary reference and default parameters. The presence of *Klebsiella* capsules was
659 assigned when the confidence level of the matches was above "good", as recommended by the
660 authors. Other capsular systems from groups I (Wzx/Wzy-dependent), II and III (ABC-dependent),
661 IV, synthase-dependent (cps3-like and hyaluronic acid) and PGA (Poly-γ-d-glutamate) were
662 searched using MacSyFinder v1.0.5 with the CapsuleFinder for diderms models, indicating
663 "ordered_replicon" as database type and linear topology (56, 61). Only systems reported as
664 complete were considered. In the cases where *Klebsiella* capsular loci were also identified by
665 CapsuleFinder as group I capsules, analyses were performed with the Kaptive output. To assess
666 the similarity of the different sets of capsular loci between strains, a weighted gene repertoire
667 relatedness (wGRR) score was calculated as in (62). For this, significant sequence similarities (e-
668 value $<10^{-4}$, identity ≥35%, coverage ≥50%) among all pairs of proteins in the capsular loci were
669 searched using MMSeqs2 (Nature Biotechnology release, August 2017, (63)) with the sensitivity
670 parameter set to 7.5. The best bi-directional hits between pairs of capsule loci sets were then
671 used to compute the wGRR as:

672 $$wGRR_{A,B} = \Sigma_i \frac{id(A_i, B_i)}{min(A, B)}$$

673 where $id(A_i, B_i)$ is the sequence identity between each pair *i* of homologous proteins in *A* and *B*,
674 and $min(A, B)$ is the number of proteins of the capsule loci set encoding the fewest proteins (*A* or
675 *B*). The wGRR takes values between 0 (no homologous proteins between capsule loci sets) and
676 1 (all genes of the smallest capsule loci set have an identical homologous in the loci set of the
677 other strain), representing the fraction of homologs in the smallest of the two capsule loci set
678 weighted by their sequence similarity. Protein sequences of the *Klebsiella* capsular loci were

679 obtained from Prokka annotations of the operon nucleotide sequences output by Kaptive. All
680 proteins between the borders of CapsuleFinder complete systems were included.

681 **Analysis of capsular systems in a database.** The database comprised the genomes of 730 *K.*
682 *pneumoniae* and 1,585 *E. coli* downloaded from the NCBI RefSeq database of high quality
683 complete non-redundant genomes (retrieved from ftp://ftp.ncbi.nlm.nih.gov/genomes/refseq/ on
684 March 2021; Table S3) (64). pOXA-48-carrying strains were identified in the RefSeq database
685 when the best, largest BLASTn hit between the sequence of pOXA-48_K8 (MT441554) and the
686 target plasmid had >95% identity and >10 Kb alignment, and when the plasmid sequence
687 contained the pOXA-48 IncL replicon and the $bla_{\text{OXA-48}}$ gene as detected by ABRicate with the
688 PlasmidFinder and ResFinder databases. The plasmids of 6 *E. coli* and 46 *K. pneumoniae* strains
689 met this criteria, which had lengths between 50.6-74.2 Kb (average 64.0 Kb; Table S3). Kaptive
690 and CapsuleFinder were used as previously described to search for *Klebsiella*-derived capsules
691 and capsular systems, respectively, and to discard non-capsulated strains (15 *K. pneumoniae*
692 strains).

693 Associations between the presence of *Klebsiella*-derived capsules and pOXA-48- or plasmid-
694 carriage were analyzed building 2x2 contingency tables. Significant interactions ($P < 0.05$, Fisher
695 exact test) were then corrected for phylogenetic dependency, i.e. the tendency of closely related
696 strains to share the same traits. For this, a set of 128 HMM profiles (Pfam release 35, Table S4)
697 of conserved bacterial single copy genes, described in (65) and curated in (66), were identified in
698 the RefSeq strains and an *Enterobacter cloacae* outgroup (accession number
699 GCF_003204095.1) using HMMER v3.3 (option --cut_ga) (67). Hits were filtered by score using
700 the cutoffs reported in (65), resulting in 127 gene markers present in >90% of strains. Protein
701 sequences of each family were aligned with MAFFT v7.453 (option --auto) (68) and alignments
702 were trimmed with trimAl v1.4.rev15 (69). IQ-TREE v1.6.12 (70) was used to infer two
703 phylogenetic trees from the concatenated alignments (the first including all capsulated strains,
704 and the second including only *E. coli* strains, both with the *E. cloacae* outgroup) with best
705 evolutionary model selection and 1000 ultrafast bootstrap. Trees were rooted and rescaled to a
706 total height of 1. Phylogenetic logistic regression for each significant association was performed
707 with the function *phyloglm* from the *phylolm* v2.6.4 R package (71), fitting a logistic MPLE model
708 with 100 independent bootstrap replicates.

Mathematical model. The plasmid population dynamics model consists of a set of differential equations describing changes in the abundance of bacterial subpopulations competing for a single limiting resource in a homogeneous environment. If the time-dependant concentration of the limiting resource is denoted by $R(t)$, then growth of each strain can be modeled as a Monod term with the following growth kinetic parameters: a maximum uptake rate (V_{max}), a half-saturation constant (K_m), and a resource conversion coefficient (ρ). Parameter values of each strain in our collection were previously obtained using a Markov chain Monte Carlo algorithm with a Metropolis-Hastings sampler (30). Convergence of the Markov chains after a burn-in period and a thinning of 100 iterations was verified by obtaining Gelman–Rubin $\hat{R}$ statistical values near one for all strains. Robustness to different priors was verified by obtaining similar maximum likelihood estimates for uniform, lognormal, gamma, and beta prior distributions. The identifiability of growth kinetic parameters was confirmed using a data cloning algorithm (72).

To model the action of a bactericidal antibiotic in each subpopulation, we explicitly considered the environmental concentration of an antibiotic with a time-dependant variable $A(t)$. Parameter α denotes the rate at which antibiotic molecules are inactivated by binding to their cellular targets, and κ the corresponding killing rate. Resistance to the antibiotic is a consequence of a reduced killing rate, resulting from encoding a resistance gene in a mobile genetic element. Therefore the model considers that each strain can be either plasmid-bearing or plasmid-free, with densities of each subpopulation denoted by B_p and $B_\emptyset$ respectively (we also use the same subindex p or $\emptyset$ to denote parameter values corresponding to plasmid-bearing or plasmid-free cells). We assume that plasmids are randomly segregated between daughter cells, so plasmid-free cells are produced from the plasmid-bearing subpopulation at a rate λ. To model horizontal gene transfer, we consider that conjugation is proportional to the densities of both donor and recipient cells. Therefore the rate of conjugation can be represented with γ, a parameter that is determined by the plasmid permissiveness of the receiving cell to pOXA-48. Then the system of differential equations that describes the population dynamics of plasmid-free and plasmid-bearing subpopulations can be written as

$$\frac{dR}{dt} = -u_p(R)B_p - u_{\varnothing}(R)B_{\varnothing} - \delta R,$$

$$\frac{dA}{dt} = -\alpha A(B_p + B_{\varnothing}) - \delta A,$$

$$\frac{dB_p}{dt} = \rho_p u_p(R)(1 - \lambda - \kappa_p A)B_p + \gamma B_p B_{\varnothing} - \delta B_p,$$

$$\frac{dB_{\varnothing}}{dt} = \rho_{\varnothing} u_{\varnothing}(R)(1 - \kappa_{\varnothing} A)B_{\varnothing} + \lambda(\rho_p u_p(R)B_p) - \gamma B_p B_{\varnothing} - \delta B_{\varnothing},$$

where δ denotes a constant dilution rate and $u(R) = \frac{V_{max}R}{K_m+R}$ denotes a resource uptake function.

Stochastic simulations of polymicrobial communities. Computer experiments were performed by numerically solving the population dynamics model for different environmental regimes and population structures. Random environments were produced in Python using a dedicated package that generates realizations of different stochastic processes, categorized under continuous, discrete, diffusion, and noise methods. To model random environments with different strengths of selection, we multiplied this stochastic time series by an amplitude parameter, $0 \leq A_{max} \leq 1$, representing the maximum selective pressure imposed by the environment. In particular, numerical experiments presented were performed with a daily drug concentration obtained with a probability density function equal to that of a Normal distribution. We repeated the experiments for environments characterized by other sources of noise and obtained qualitatively the same distribution of plasmids in the population.

Polyclonal communities of M individuals were assembled by randomly sampling M<N individuals from our collection of N=20 strains (10 Ec and 10 Kpn). If we denote with B_p^i and $B_{\varnothing}^i$ the densities of plasmid-bearing and plasmid-free subpopulations of strain i, then the bacterial community can be represented with vector $B(t) = (B_p^1(t), B_p^2(t), \ldots, B_p^M(t), B_{\varnothing}^1(t), B_{\varnothing}^2(t), \ldots, B_{\varnothing}^M(t))$. As all cells consume the limiting resource at a rate determined by their corresponding growth kinetic parameters, then the equation that describes the rate of change of resource R can be written as

$$\frac{dR}{dt} = -\sum_{i=1}^{M} \left(u_p^i(R(t)) \cdot B_p^i(t) + u_{\varnothing}^i(R(t)) \cdot B_{\varnothing}^i(t)\right) - \delta R.$$

761 We assume that antibiotic molecules are inactivated at a rate that is proportional to the total
762 bacterial population and the environmental drug concentration,

763 $$\frac{dA}{dt} = -\alpha A(t) \sum_{i=1}^{M} (B_p^i(t) + B_\varnothing^i(t)) - \delta A.$$

764 As the model considers that plasmid conjugation is restricted by the receiving cell, then we denote
765 with γ^i the permissiveness of strain i towards pOXA-48. Therefore bacterial growth of the plasmid-
766 bearing subpopulation of strain i depends on the contribution of all plasmid-bearing populations,

767 $$\frac{dB_p^i}{dt} = \rho_p^i u_p^i(R)(1 - \lambda - \kappa_p^i A) \cdot B_p^i + \gamma^i B_\varnothing^i \cdot \sum_{j=1}^{M} B_p^j - \delta B_p^i .$$

768 Similarly, the population dynamics of plasmid-free strain i can be written as

769 $$\frac{dB_\varnothing^i}{dt} = \rho_\varnothing u_\varnothing(R)(1 - \kappa_\varnothing A)B_\varnothing^i + \lambda(\rho_p u_p(R)B_p^i) - \gamma^i B_\varnothing^i \sum_{j=1}^{M} B_p^j - d\delta.$$

770 Initial conditions of competition experiments assumed that all strains in the community, both with
771 and without plasmid, were present at equal initial densities at time $t = 0$. For plasmid invasion
772 experiments, we considered a community of plasmid-free cells, with 0.1% of cells of a random
773 strain carrying plasmids. Computer simulations were implemented in Matlab using standard
774 numerical solvers and scientific libraries. All code and data used is available at
775 https://github.com/ccg-esb/EvK.

776 **Statistical analyses.** All statistical analyses were performed with R v4.2.2 (www.R-project.org).
777 Packages *ggplot2* v3.3.6, *ggpubr* v0.4.0 *pheatmap* v1.0.12, *RColorBrewer* v1.1-3, *ggsignif* v0.6.3
778 and *tidyverse* v1.3.1 were used for data manipulation and representation. R base packages were
779 used for statistical tests. Normality of the data was assessed with the Shapiro-Wilk test. To
780 analyze the differences in initial (PF) and final (TC) MIC of antibiotics and PCN between *E. coli*
781 and *Klebsiella* spp. a Wilcoxon sum-rank test was used. To analyze the differences between the
782 members of each recipient couple in the pairwise conjugation experiments (Shapiro-Wilk
783 normality test, $P < 0.01$ in all cases), the non-parametric Wilcoxon paired signed-rank test was
784 used. To determine differences between receptor species in the classical and pooled recipient
785 conjugation experiments, as well as in *in vivo* conjugation assays (Shapiro-Wilk normality test, *P*

786 < 0.01 in all cases), the non-parametric Kruskal-Wallis test was performed. Correlations were
787 performed with the Spearman's rank test. Phylogenetic analyses were performed with *ape* v5.6-
788 2, *phytools* v1.0-3 and *phylolm* v2.6.4 packages.

789 **Data and code availability.** Sequencing data generated in this study is available in the Sequence
790 Read Archive (SRA) under the BioProject PRJNA803387. The R-GNOSIS sequences were
791 generated in (28) and a subset of strains were selected as in (32) (see Methods). Source data is
792 provided. The code generated during the study along with detailed bioinformatic methods is
793 available at https://github.com/LaboraTORIbio/super-sinks.

794 **Acknowledgements**

795 We thank J. Penadés for constructive comments. This work was supported by the European
796 Research Council (ERC) under the European Union's Horizon 2020 research and innovation
797 programme (ERC grant no. 757440-PLASREVOLUTION) and by the Instituto de Salud Carlos III
798 (PI19/00749) cofunded by the European Development Regional Fund 'A way to achieve Europe'.
799 The R-GNOSIS project received financial support from the European Commission (grant no. R-
800 GNOSIS-F P7-HEALTH-F3-2011-282512). C.U. was supported by a grant from MICINN
801 (PID2020-120292RB-I00). R.P.M. and C.T.P. received funding from CONACYT Ciencia Basica
802 (grant A1-S-321649). C.T.P: also received funding from CONACYT Fronteras (grant 2019-
803 217367).

Bibliography

1. J. P. Gogarten, J. P. Townsend, Horizontal gene transfer, genome innovation and evolution. Nat Rev Microbiol 3, 679–687 (2005).
2. A. San Millan, R. C. MacLean, Fitness Costs of Plasmids: a Limit to Plasmid Transmission. Microbiol. Spectr. 5 (2017).
3. D. A. Baltrus, Exploring the costs of horizontal gene transfer. Trends Ecol Evol 28, 489–495 (2013).
4. K. Z. Coyte, et al., Horizontal gene transfer and ecological interactions jointly control microbiome stability. PLOS Biol. 20, e3001847 (2022).
5. M. A. Brockhurst, E. Harrison, Ecological and evolutionary solutions to the plasmid paradox. Trends Microbiol. (2021) https:/doi.org/10.1016/j.tim.2021.11.001.
6. M. J. Bottery, Ecological dynamics of plasmid transfer and persistence in microbial communities. Curr. Opin. Microbiol. 68, 102152 (2022).
7. F. M. Stewart, B. R. Levin, The Population Biology of Bacterial Plasmids: A PRIORI Conditions for the Existence of Conjugationally Transmitted Factors. Genetics 87, 209–228 (1977).
8. A. J. Lopatkin, et al., Persistence and reversal of plasmid-mediated antibiotic resistance. Nat. Commun. 8, 1689 (2017).
9. P. E. Turner, V. S. Cooper, R. E. Lenski, TRADEOFF BETWEEN HORIZONTAL AND VERTICAL MODES OF TRANSMISSION IN BACTERIAL PLASMIDS. Evol. Int. J. Org. Evol. 52, 315–329 (1998).
10. J. H. Bethke, et al., Vertical and horizontal gene transfer tradeoffs direct plasmid fitness. Mol. Syst. Biol., e11300 (2022).
11. F. Benz, A. R. Hall, “Host-specific plasmid evolution explains the variable spread of clinical antibiotic-resistance plasmids” (Evolutionary Biology, 2022) https:/doi.org/10.1101/2022.07.06.498992 (January 3, 2023).
12. Jordt, H., et al. Coevolution of host–plasmid pairs facilitates the emergence of novel multidrug resistance. Nat. Ecol. Evol. 4, 863–869 (2020)
13. C. T. Bergstrom, M. Lipsitch, B. R. Levin, Natural selection, infectious transfer and the existence conditions for bacterial plasmids. Genetics 155, 1505–1519 (2000).
14. L. N. Lili, N. F. Britton, E. J. Feil, The persistence of parasitic plasmids. Genetics 177, 399–405 (2007).
15. J. M. Ponciano, L. De Gelder, E. M. Top, P. Joyce, The population biology of bacterial plasmids: a hidden Markov model approach. Genetics 176, 957–968 (2007).
16. J. C. R. Hernández-Beltrán, A. San Millán, A. Fuentes-Hernández, R. Peña-Miller, Mathematical Models of Plasmid Population Dynamics. Front. Microbiol. 12, 3389 (2021).
17. A. San Millan, et al., Positive selection and compensatory adaptation interact to stabilize non-transmissible plasmids. Nat Commun 5, 5208 (2014).
18. J. P. J. Hall, A. J. Wood, E. Harrison, M. A. Brockhurst, Source–sink plasmid transfer dynamics maintain gene mobility in soil bacterial communities. Proc. Natl. Acad. Sci. 113, 8260–8265 (2016).
19. L. Li, et al., Plasmids persist in a microbial community by providing fitness benefit to multiple phylotypes. ISME J. 14, 1170–1181 (2020).
20. T. Dimitriu, L. Marchant, A. Buckling, B. Raymond, Bacteria from natural populations transfer plasmids mostly towards their kin. Proc. R. Soc. B 286, 20191110 (2019).
21. J. H. Bethke, et al., Environmental and genetic determinants of plasmid mobility in pathogenic *Escherichia coli*. Science Advances. 6, 4 (2020).
22. S. R. Partridge, S. M. Kwong, N. Firth, S. O. Jensen, Mobile genetic elements associated with antimicrobial resistance. Clin. Microbiol. Rev. 31 (2018).
23. C. J. L. Murray, et al., Global burden of bacterial antimicrobial resistance in 2019: a systematic analysis. The Lancet (2022) https:/doi.org/10.1016/S0140-6736(21)02724-0.
24. WHO, List of bacteria for which new antibiotics are urgently needed

857 https://www.who.int/news/item/27-02-2017-who-publishes-list-of-bacteria-for-which-new-
858 antibiotics-are-urgently-needed (January 3, 2023).
859 25. A. Cassini, et al., Attributable deaths and disability-adjusted life-years caused by infections
860 with antibiotic-resistant bacteria in the EU and the European Economic Area in 2015: a
861 population-level modelling analysis. Lancet Infect. Dis. 19, 56–66 (2019).
862 26. J. D. D. Pitout, G. Peirano, M. M. Kock, K.-A. Strydom, Y. Matsumura, The Global
863 Ascendency of OXA-48-Type Carbapenemases. Clin. Microbiol. Rev. 33, e00102-19 (2019).
864 27. S. Redondo-Salvo, et al., Pathways for horizontal gene transfer in bacteria revealed by a
865 global map of their plasmids. Nat. Commun. 11, 3602 (2020).
866 28. R. León-Sampedro, et al., Pervasive transmission of a carbapenem resistance plasmid in the
867 gut microbiota of hospitalized patients. Nat. Microbiol. 6, 606–616 (2021).
868 29. S. David, et al., Epidemic of carbapenem-resistant Klebsiella pneumoniae in Europe is
869 driven by nosocomial spread. Nat. Microbiol. 4, 1919–1929 (2019).
870 30. A. Alonso-del Valle, et al., Variability of plasmid fitness effects contributes to plasmid
871 persistence in bacterial communities. Nat. Commun. 12, 2653 (2021).
872 31. A. San Millan, J. A. Escudero, D. R. Gifford, D. Mazel, R. C. MacLean, Multicopy plasmids
873 potentiate the evolution of antibiotic resistance in bacteria. Nat. Ecol. Evol. 1, 10 (2016).
874 32. J. DelaFuente, et al., Within-patient evolution of plasmid-mediated antimicrobial resistance.
875 Nat. Ecol. Evol. 6, 1980–1991 (2022).
876 33. R. Fernandez-Lopez, I. del Campo, C. Revilla, A. Cuevas, F. de la Cruz, Negative Feedback
877 and Transcriptional Overshooting in a Regulatory Network for Horizontal Gene Transfer.
878 PLoS Genet. 10, e1004171 (2014).
879 34 A. Djukovic, et al., Lactobacillus supports Clostridiales to restrict gut colonization by
880 multidrug- resistant Enterobacteriaceae. (2022). Nat. Commun. 13, 5617 (2022).
881 35. M. Haudiquet, A. Buffet, O. Rendueles, E. P. C. Rocha, Interplay between the cell envelope
882 and mobile genetic elements shapes gene flow in populations of the nosocomial pathogen
883 Klebsiella pneumoniae. PLoS Biol. 19, e3001276 (2021).
884 36. C. Brehony, et al., An MLST approach to support tracking of plasmids carrying OXA-48-like
885 carbapenemase. J. Antimicrob. Chemother. 74, 1856–1862 (2019).
886 37. A. M. Hammerum, et al., Investigation of possible clonal transmission of carbapenemase-
887 producing Klebsiella pneumoniae complex member isolates in Denmark using core genome
888 MLST and National Patient Registry Data. Int. J. Antimicrob. Agents 55, 105931 (2020).
889 38. H. Arabaghian, et al., Molecular Characterization of Carbapenem Resistant Klebsiella
890 pneumoniae and Klebsiella quasipneumoniae Isolated from Lebanon. Sci. Rep. 9, 531
891 (2019).
892 39. A. K. Brödel, et al., In situ targeted mutagenesis of gut bacteria. bioRxiv, 2022.09.30.509847
893 (2022).
894 40. R. López-Igual, J. Bernal-Bayard, A. Rodríguez-Patón, J.-M. Ghigo, D. Mazel, Engineered
895 toxin-intein antimicrobials can selectively target and kill antibiotic-resistant bacteria in mixed
896 populations. Nat. Biotechnol. 37, 755–760 (2019).
897 41. F. Le Roux, J. Binesse, D. Saulnier, D. Mazel, Construction of a Vibrio splendidus Mutant
898 Lacking the Metalloprotease Gene vsm by Use of a Novel Counterselectable Suicide Vector.
899 Appl. Environ. Microbiol. 73, 777–784 (2007).
900 42. I. Wiegand, K. Hilpert, R. E. W. Hancock, Agar and broth dilution methods to determine the
901 minimal inhibitory concentration (MIC) of antimicrobial substances. Nat. Protoc. 3, 163–175
902 (2008).
903 43. M. Agarwal, R. S. Rathore, A. Chauhan, A Rapid and High Throughput MIC Determination
904 Method to Screen Uranium Resistant Microorganisms. Methods Protoc. 3, 21 (2020).
905 44. M. Carlier, A. G. Verstraete, J. J. De Waele, V. Stove, Stability of amoxicillin and
906 amoxicillin/clavulanic acid reconstituted in isotonic saline. J. Chemother. 29, 54–56 (2017).
907 45. A. Bankevich, et al., SPAdes: a new genome assembly algorithm and its applications to
908 single-cell sequencing. J. Comput. Biol. J. Comput. Mol. Cell Biol. 19, 455–477 (2012).
909 46. A. Gurevich, V. Saveliev, N. Vyahhi, G. Tesler, QUAST: quality assessment tool for genome

910 assemblies. Bioinforma. Oxf. Engl. 29, 1072–1075 (2013).
911 47. L. S. Katz, et al., Mashtree: a rapid comparison of whole genome sequence files. J. Open
912 Source Softw. 4, 1762 (2019).
913 48. H. Wang, et al., Increased plasmid copy number is essential for Yersinia T3SS function and
914 virulence. Science 353, 492–495 (2016).
915 49. P. K. Jangir, et al., Pre-existing chromosomal polymorphisms in pathogenic E. coli potentiate
916 the evolution of resistance to a last-resort antibiotic. eLife 11, e78834 (2022).
917 50. H. Li, Aligning sequence reads, clone sequences and assembly contigs with BWA-MEM
918 (2013) https:/doi.org/10.48550/arXiv.1303.3997 (January 18, 2023).
919 51. P. Danecek, et al., Twelve years of SAMtools and BCFtools. GigaScience 10, giab008
920 (2021).
921 52. T. Seemann, Prokka: rapid prokaryotic genome annotation. Bioinformatics 30, 2068–2069
922 (2014).
923 53. R. J. Roberts, T. Vincze, J. Posfai, D. Macelis, REBASE—a database for DNA restriction
924 and modification: enzymes, genes and genomes. Nucleic Acids Res. 38, D234–D236 (2010).
925 54. S. F. Altschul, W. Gish, W. Miller, E. W. Myers, D. J. Lipman, Basic local alignment search
926 tool. J. Mol. Biol. 215, 403–410 (1990).
927 55. P. H. Oliveira, M. Touchon, E. P. C. Rocha, Regulation of genetic flux between bacteria by
928 restriction–modification systems. Proc. Natl. Acad. Sci. 113, 5658–5663 (2016).
929 56. S. S. Abby, B. Néron, H. Ménager, M. Touchon, E. P. C. Rocha, MacSyFinder: a program to
930 mine genomes for molecular systems with an application to CRISPR-Cas systems. PLOS
931 ONE 9, e110726 (2014).
932 57. F. Tesson, et al., Systematic and quantitative view of the antiviral arsenal of prokaryotes.
933 Nat. Commun. 13, 2561 (2022).
934 58. L. J. Payne, et al., Identification and classification of antiviral defence systems in bacteria
935 and archaea with PADLOC reveals new system types. Nucleic Acids Res. 49, 10868–10878
936 (2021).
937 59. S. S. Abby, et al., Identification of protein secretion systems in bacterial genomes. Sci. Rep.
938 6, 23080 (2016).
939 60. M. M. C. Lam, R. R. Wick, L. M. Judd, K. E. Holt, K. L. Wyres, Kaptive 2.0: updated capsule
940 and lipopolysaccharide locus typing for the Klebsiella pneumoniae species complex. Microb.
941 Genomics 8, 000800 (2022).
942 61. O. Rendueles, M. Garcia-Garcerà, B. Néron, M. Touchon, E. P. C. Rocha, Abundance and
943 co-occurrence of extracellular capsules increase environmental breadth: Implications for the
944 emergence of pathogens. PLOS Pathog. 13, e1006525 (2017).
945 62. J. A. M. de Sousa, A. Buffet, M. Haudiquet, E. P. C. Rocha, O. Rendueles, Modular
946 prophage interactions driven by capsule serotype select for capsule loss under phage
947 predation. ISME J. 14, 2980–2996 (2020).
948 63. M. Steinegger, J. Söding, MMseqs2 enables sensitive protein sequence searching for the
949 analysis of massive data sets. Nat. Biotechnol. 35, 1026–1028 (2017).
950 64. D. H. Haft, et al., RefSeq: an update on prokaryotic genome annotation and curation. Nucleic
951 Acids Res. 46, D851–D860 (2018).
952 65. C. Rinke, et al., Insights into the phylogeny and coding potential of microbial dark matter.
953 Nature 499, 431–437 (2013).
954 66. C. d'Humières, et al., A simple, reproducible and cost-effective procedure to analyse gut
955 phageome: from phage isolation to bioinformatic approach. Sci. Rep. 9, 11331 (2019).
956 67. S. R. Eddy, Accelerated Profile HMM Searches. PLOS Comput. Biol. 7, e1002195 (2011).
957 68. K. Katoh, D. M. Standley, MAFFT Multiple Sequence Alignment Software Version 7:
958 Improvements in Performance and Usability. Mol. Biol. Evol. 30, 772–780 (2013).
959 69. S. Capella-Gutiérrez, J. M. Silla-Martínez, T. Gabaldón, trimAl: a tool for automated
960 alignment trimming in large-scale phylogenetic analyses. Bioinforma. Oxf. Engl. 25, 1972–
961 1973 (2009).
962 70. L.-T. Nguyen, H. A. Schmidt, A. von Haeseler, B. Q. Minh, IQ-TREE: A Fast and Effective

Stochastic Algorithm for Estimating Maximum-Likelihood Phylogenies. Mol. Biol. Evol. 32, 268–274 (2015).

71. L. si Tung Ho, C. Ané, A linear-time algorithm for Gaussian and non-Gaussian trait evolution models. Syst. Biol. 63, 397–408 (2014).
72. S. R. Lele, B. Dennis, F. Lutscher, Data cloning: easy maximum likelihood estimation for complex ecological models using Bayesian Markov chain Monte Carlo methods. Ecol Lett 10, 551–563 (2007).

972 **Supplementary Figures**

973

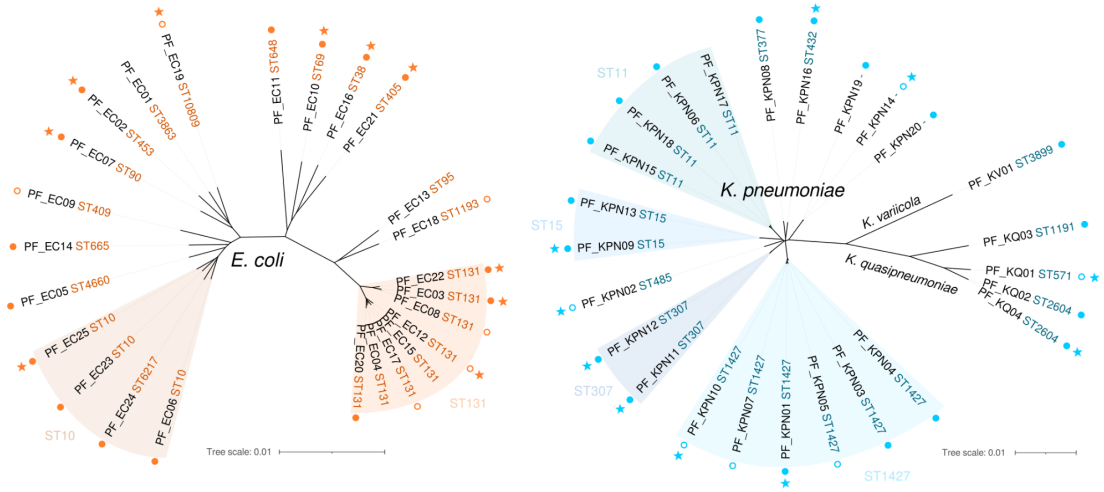

974

975 **Fig. S1.** Unrooted phylogeny of *E. coli* (left, n=25) and *Klebsiella* spp. (right, n=25) plasmid-free
976 (PF) strains. Branch lengths represent mash distances between the whole-genome assemblies
977 of the strains. Groups of strains belonging to the same multilocus sequence type (ST) are shaded
978 (note that *E. coli* ST6217 is part of the ST10 group). Filled circles indicate strains for which
979 transconjugants (TC) with an isogenic pOXA-48 could be obtained and were therefore used to
980 determine minimum inhibitory concentrations (MIC) to antibiotics and pOXA-48 copy number (*E.*
981 *coli* n=15, *Klebsiella* spp. n=18). Empty circles indicate that TC could be obtained but harbored a
982 mutated pOXA-48 plasmid. PF strains used as recipients in conjugation experiments are marked
983 with a star.

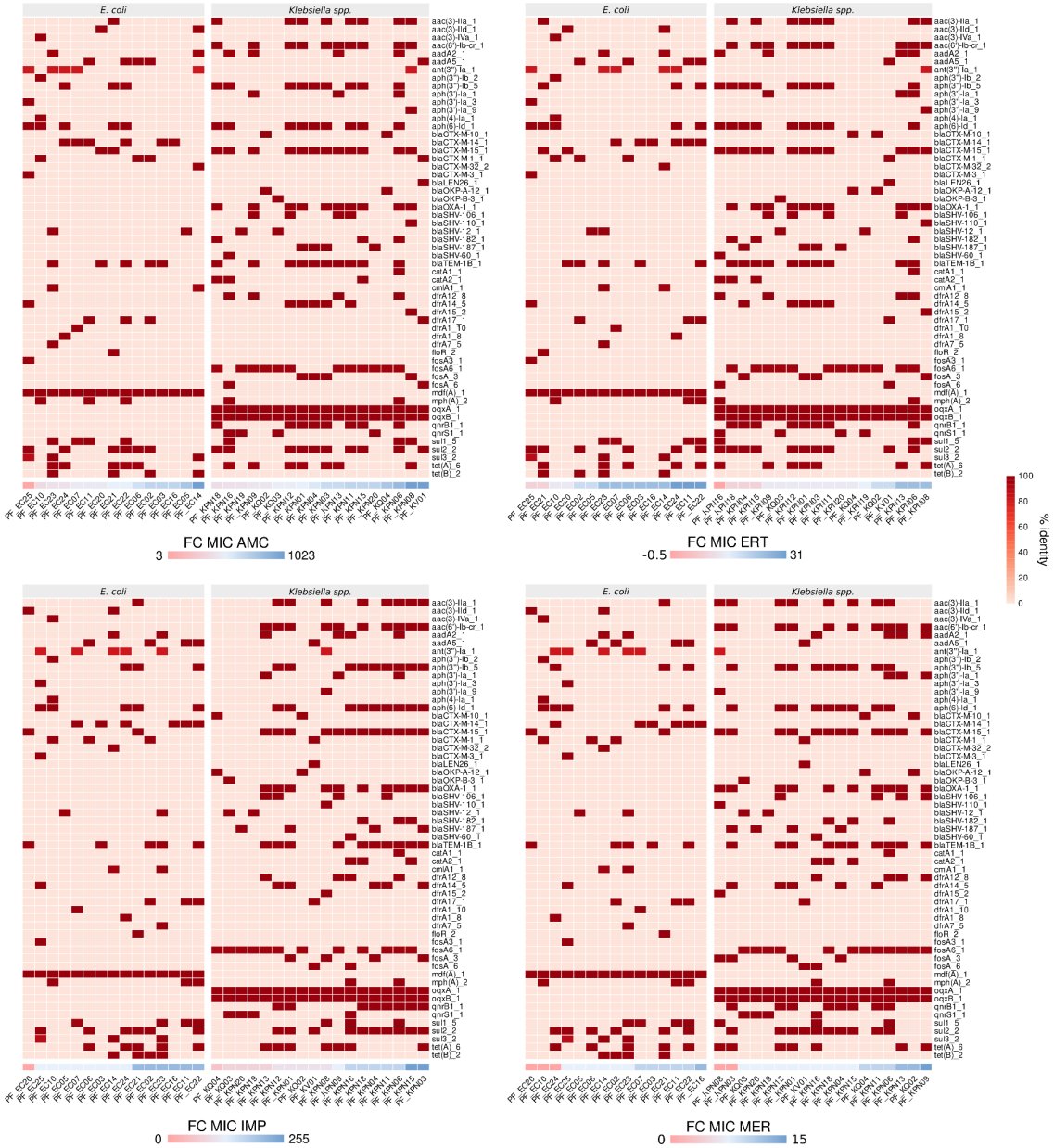

Fig. S2. Antimicrobial resistance (AMR) genes encoded by the plasmid-free (PF) strains used to determine minimum inhibitory concentrations (MICs) to antibiotics. The heatmap shows presence (colored by percentage of identity to the BLAST hit in the ResFinder database; see Methods) and absence (values of 0) of the AMR genes. In each of the four panels, the PF strains are ordered by fold change (FC) in MIC to the corresponding antibiotic when acquiring pOXA-48 (top left, amoxicillin/clavulanic acid, AMC; top right, ertapenem, ERT; bottom left, imipenem, IMP; bottom right, meropenem, MER).

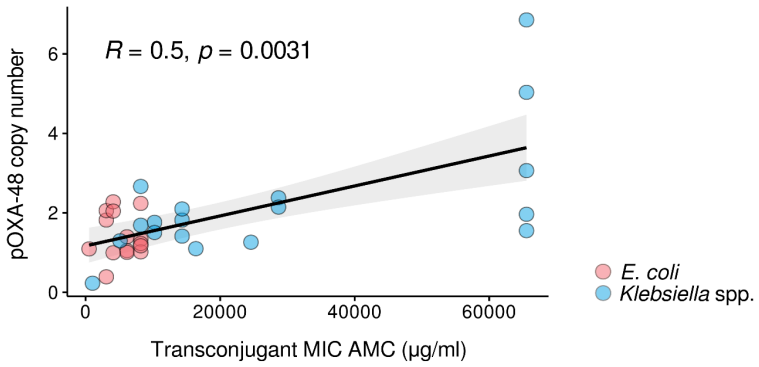

993
994

995 **Fig. S3.** Spearman's correlation between pOXA-48 copy number and the minimum inhibitory
996 concentration (MIC) of amoxicillin/clavulanic acid (AMC) in the pOXA-48-carrying clones. pOXA-
997 48 copy number was estimated from sequencing data as the ratio of plasmid/chromosome median
998 coverage (see Methods).

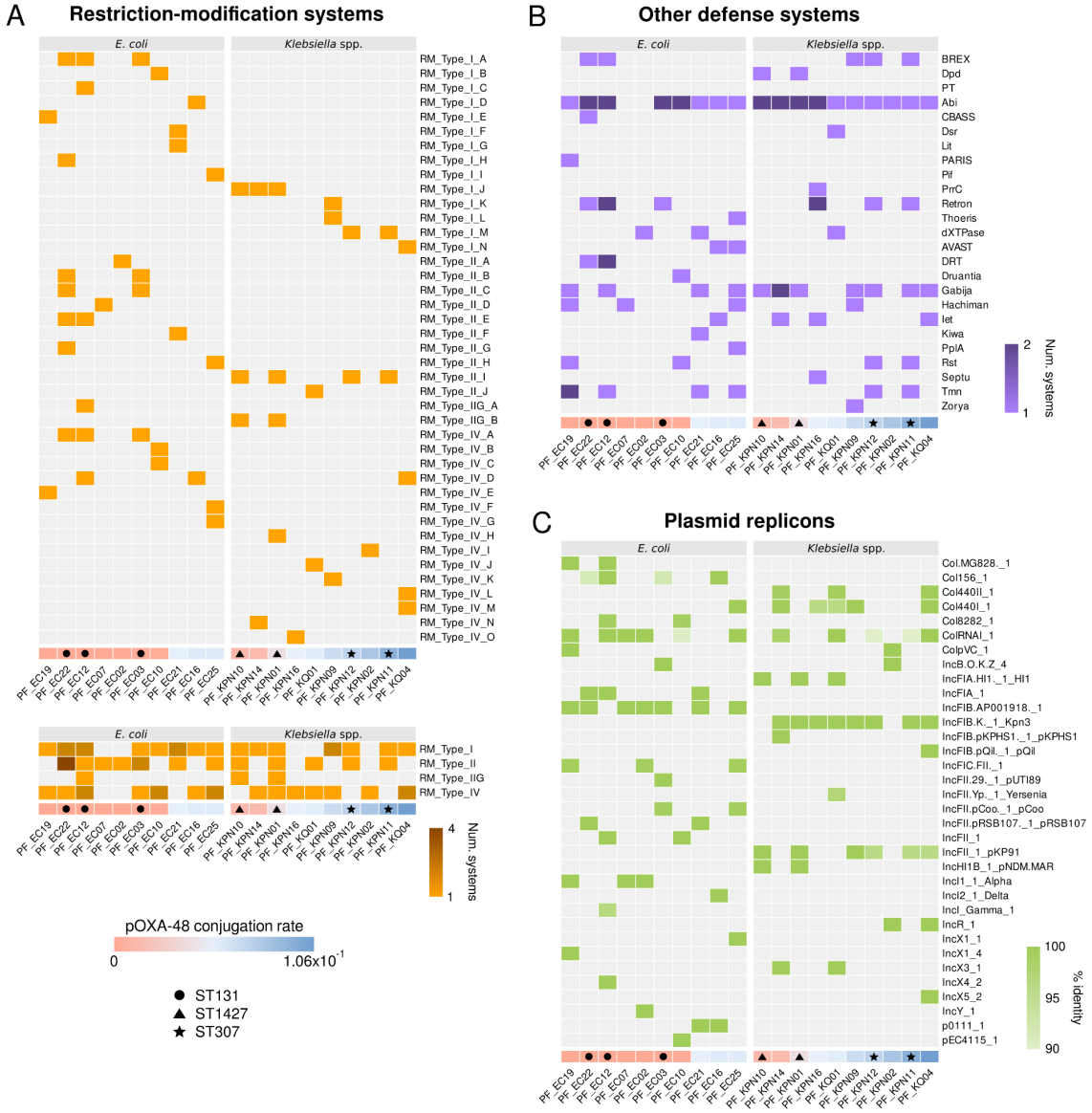

Fig. S4. Analysis of genomic traits in recipient strains that could explain differences in pOXA-48 acquisition by conjugation. (A) Heatmap of presence/absence of restriction-modification (RM) systems. In the top panel, all RM systems subtypes, labeled with different letters, are shown. In the bottom panel, RM systems are collapsed by type. (B) Heatmap of presence/absence of other phage defense systems. (C) Heatmap of presence/absence of plasmid replicons. The intensity of the color scale in A bottom and B indicate the number of systems of a specific type a strain is encoding, while in C indicates the percentage of identity of the replicon to the BLAST hit of the PlasmidFinder database (see Methods). In A-C, recipient strains are ordered by mean pOXA-48 conjugation rates across replicates and experimental conditions. Strains belonging to the same sequence type (ST) are marked with a symbol.

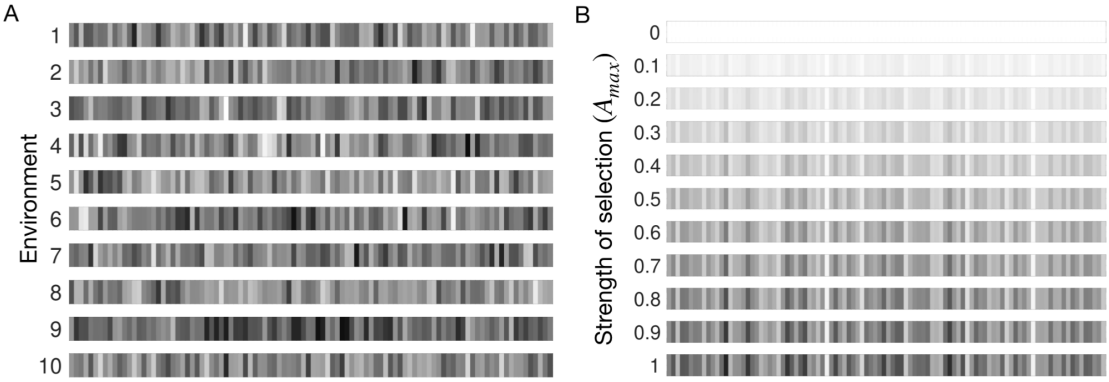

Fig. S5. Stochastic environments used in numerical experiments. (A) Each row depicts a unique environmental condition that changes daily, with the drug concentration based on a Gaussian probability density function. Drug concentration is indicated using shades of gray. (B) Each row displays a stochastic environmental condition with increasing levels of selection strength ($0 \leq A_{max} \leq 1$).

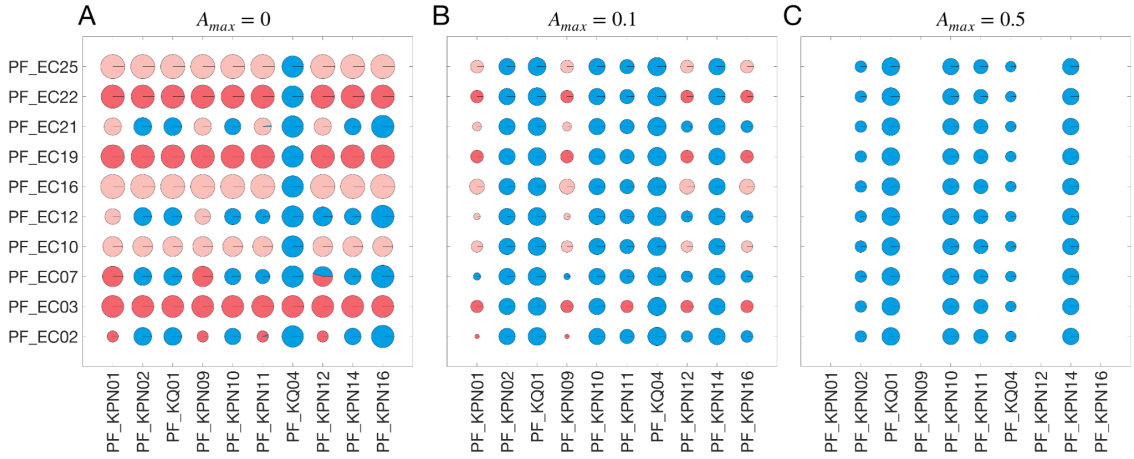

Fig. S6. Pairwise competition experiments between *E. coli* and *Klebsiella* spp. strains. (A) In a drug-free environment ($A_{max} = 0$). The diameter of each circle is proportional to the total bacterial density observed at the end of the experiment. Plasmid-free and plasmid-bearing subpopulations are denoted with light and dark colors, respectively (*Klebsiella* spp. in blue and *E. coli* in red). (B) In the presence of antibiotics ($A_{max} = 0.1$), plasmid-bearing *Klebsiella* spp. strains outcompete most *E. coli* strains. (C) At high drug concentrations ($A_{max} = 0.5$), only highly resistant *Klebsiella* spp. strains are present at the end of the experiment.

1029
1030

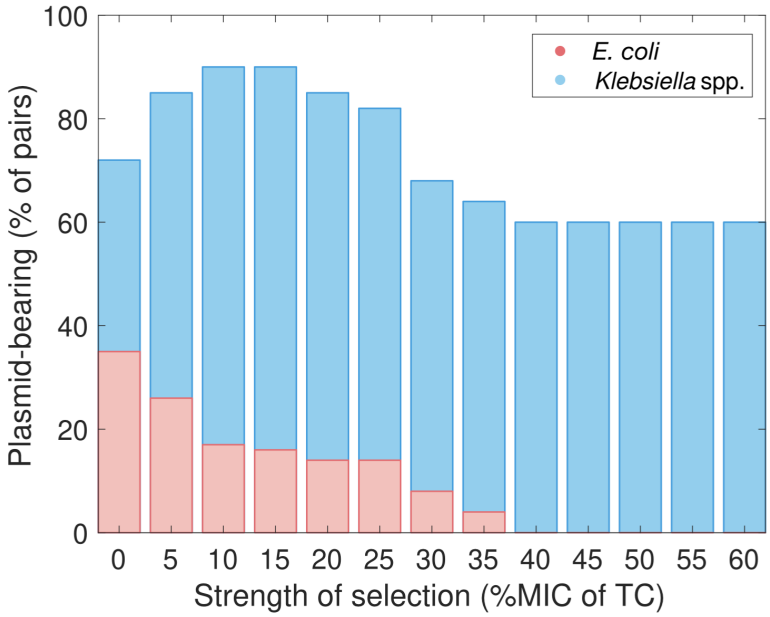

1031
1032
1033 **Fig. S7.** Percentage of pairwise *E. coli* / *Klebsiella* spp. associations where the plasmid remains
1034 stable over time. The red bars indicate the cases where the plasmid was present in the *E. coli*
1035 strains, and the blue bars indicate those cases where the plasmid was maintained in the *Klebsiella*
1036 spp. strain. Note that the presence of plasmids is highest at intermediate strengths of selection,
1037 which corresponds to drug concentrations that select for drug-resistant *Klebsiella* spp. and *E. coli*
1038 strains.

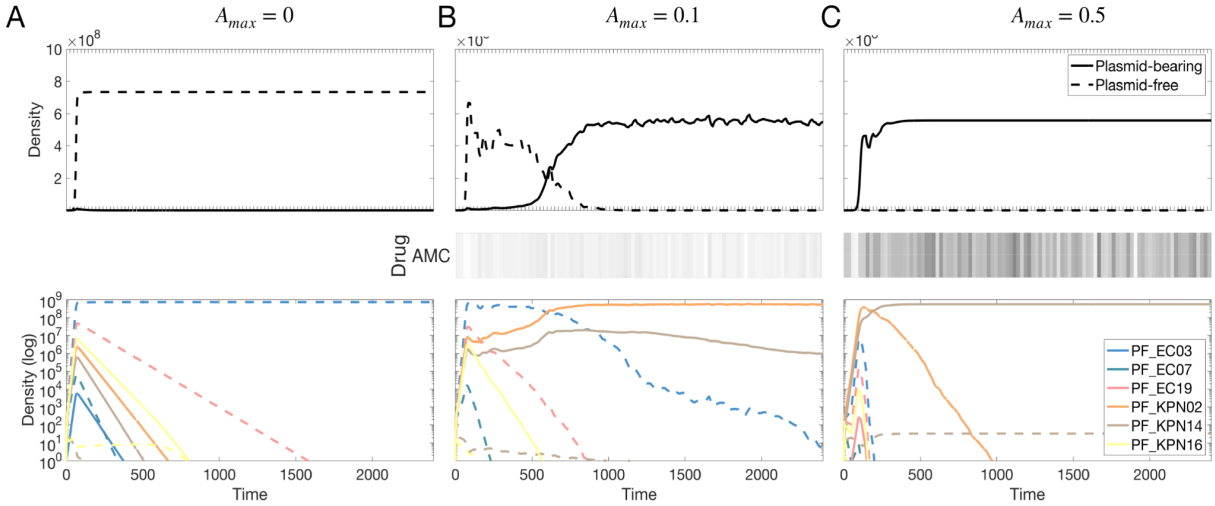

Fig. S8. Example numerical simulations for plasmid invasion in a community composed of six strains. (A) In a drug-free environment ($A_{max} = 0$), the plasmid-bearing population is outcompeted by plasmid-free cells and thus the plasmid is cleared from the population. Top plot illustrates the bacterial density at the end of each day, with dashed lines representing plasmid-free cells and solid lines representing plasmid-bearing cells. Bottom plot illustrates the density (in log scale) of each strain in the community. (B) The plasmid is stably maintained in the population in the presence of positive selection ($A_{max} = 0.1$). The drug concentration used each day is represented in the ribbon between the panels (drug concentration is shown in tones of gray). (C) Density of different strains in a stochastic environment with high levels of selection ($A_{max} = 0.5$).

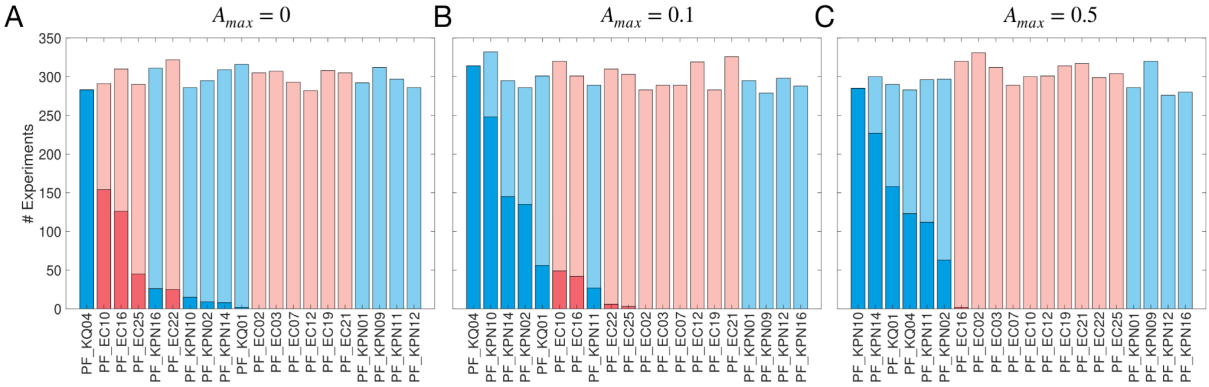

Fig. S9. Strain-level results obtained after performing 1,000 simulations of a plasmid invasion experiment in a community composed of six individuals. Each column represents a different bacterial strain (*Klebsiella* spp. in blue and *E. coli* in red). In light colors, the number of times each strain was randomly selected for the stochastic simulations. The number of experiments where the corresponding plasmid-bearing strain was detected at the end of the numerical experiment is represented with a dark bar. Strains are ordered based on the frequency of plasmid-bearing in decreasing order. (A) In drug-free environments ($A_{max} = 0$), plasmid-bearing strains can be found both in *E. coli* and *Klebsiella* spp. strains. (B) In the presence of antibiotics ($A_{max} = 0.1$), most plasmid-bearing strains are *Klebsiella* spp. strains. (C) At high drug concentrations, $A_{max} = 0.5$, all *E. coli* strains are driven to extinction and the plasmid is only present in *Klebsiella* spp. strains.